# UNIVERSITÀ DEGLI STUDI DI TRIESTE

## XXXIV CICLO DEL DOTTORATO DI RICERCA IN

## NANOTECNOLOGIE

# Label-free Surface Enhanced Raman Scattering substrates development and characterization for biofluids analysis and biomedical applications

Settore scientifico-disciplinare: chim/07

DOTTORANDO
**ALESSANDRO ESPOSITO**

COORDINATORE
**PROF. ALBERTO MORGANTE**

SUPERVISORE DI TESI
**PROF. VALTER SERGO**

TUTORE
**PROF. ALOIS BONIFACIO**

**ANNO ACCADEMICO 2021/2022**

# Riassunto

La spettroscopia Raman amplificata da superfici SERS (dall'inglese) è una potente tecnica analitica, in cui sono combinati l'elevata sensibilità e il riconoscimento delle specie chimiche, forniti rispettivamente dall'aumento del segnale di superficie e dal *finge printing* vibrazionale della spettroscopia Raman. Pertanto, lo scattering anelastico (o Raman scattering) della luce viene utilizzato per catturare le cosiddette vibrazioni attive Raman in presenza di una fonte di luce esterna. Sulla base di questo fenomeno, una vibrazione unica può consentire di identificare con elevata selettività un numero enorme di strutture chimiche. Ma la dispersione Raman è di per sé un evento raro, che si verifica solo quando si ottengono determinate circostanze. Nella spettroscopia SERS gli elettroni conduttivi oscillanti coerenti sulla superficie del metallo vengono utilizzati per amplificare l'energia vibrazionale mediante la produzione di un campo elettromagnetico molto confinato su scala nanometrica, fornendo un segnale di esito fino a 10 volte più forte di quello iniziale. Ci riferiamo a questo effetto come risonanza plasmonica di superficie localizzata LSPR, che consente a specifiche superfici nanostrutturate di raggiungere anche la risoluzione molecolare. SERS è anche una tecnica veloce e facile da usare, in cui queste caratteristiche, unite al progresso nell'ottica e nella fotonica (oggi è possibile acquistare strumentazione da banco, potabile e palmare) hanno creato un campo fertile per la diffusione delle applicazioni SERS. Tuttavia, superfici plasmoniche, o più propriamente dette substrati SERS, possono essere ottenute con una semplice procedura, ad esempio ricoprendo sulla carta nanoparticelle di argento, ottenute con riduzione di sale in acqua. Alla fine, la spettroscopia SERS è una tecnica non distruttiva che consente la misurazione in mezzi acquosi. Per tutte queste caratteristiche è stato introdotto SERS, come uno strumento promettente nella medicina di precisione e nell'analisi dei biofluidi. In questo contesto, lo scopo della mia tesi è stato quello di trovare un metodo semplice ed economico per estrarre informazioni biochimiche da matrici biologiche complesse. Il modo più semplice per eseguire le analisi biologiche SERS è utilizzare l'approccio SERS label-free. Pertanto, è possibile, in base alle composizioni del campione e all'affinità per la superficie del metallo, identificare piccole molecole e più specificamente metaboliti. Ciò fornisce un'istantanea di un pool di metaboliti di cui la variazione può essere utilizzata per

estrarre informazioni sullo stato di malattia dei pazienti. Ad esempio, molti studi sulla SERS label-free hanno raggiunto risultati interessanti come nel monitoraggio della finestra terapeutica e nella classificazione dello stato di malattia dei pazienti sulla base della concentrazione relativa di piccoli metaboliti. In questo contesto ho sviluppato per il mio progetto di dottorato, un protocollo per estrarre informazioni biochimiche da campioni di feci che sono stati adottati per studiare per la prima volta campioni di feci del paziente celiaco (la malattia celiaca può essere definita come una risposta immunogenica incontrollata al glutine ingestione), con risultati promettenti nella valutazione della compliance del paziente in dieta priva di glutine. D'altra parte, abbiamo sviluppato un protocollo di campionamento SERS veloce per siero umano sulla carta che consente di ottenere spettri SERS riproducibili tramite la centrifugazione di pochi µl di campioni individuati sulla carta in presenza di nanoparticelle colloidali d'argento. In questo modo è stato possibile ottenere un protocollo SERS veloce e affidabile da adottare per il campionamento e la bioanalitica.

# Index

Riassunto ..... 3

Abstract ..... 8

1. Rationale and background ..... 10

Bibliography ..... 13

2. Raman and SERS spectroscopy ..... 14

2.1. Raman spectroscopy ..... 14

Discovery of Raman scattering ..... 14

The Raman scattering ..... 14

Molecular vibrations ..... 16

Molecular vibrations scattering and polarizability ..... 18

The concept of selection rules ..... 22

2.2 Surface Enhanced Raman Spectroscopy ..... 24

Historical background and general principles ..... 24

Theoretical aspect ..... 26

2.3 SERS and the label-free approach for biosensing ..... 30

Bibliography ..... 31

3. label free SERS for spectroscopic investigation on stool samples: the case of study of coeliac disease ..... 34

3.1 introduction ..... 34

3.2 Experimental part ..... 37

Reagents ..... 37

Faecal samples ..... 37

SERS measurements ..... 38

SERS data pre-processing and analysis ..... 39

Genomic Analysis ..... 40

Genomic data pre-processing and analysis ..... 40

3.3 Result and discussion ..... 40

3.4 conclusions ..... 48

Bibliography ..... 49

4. A protocol study on human serum for Label free SERS biosensing: the centrifugal silver plasmonic paper (CSPP) sampling methodology ..... 54
4.1Introduction: ..... 54
4.2 Experimental section ..... 58
Materials and regents ..... 58
Silver nanoparticle Synthesis and characterization ..... 58
Serum filtration protocol ..... 58
Protocol for CSPP sampling methodology ..... 59
SERS spectral acquisition and data processing. ..... 59
Serum collecting system shelf-life ..... 60
Linear regression model and method optimization ..... 60
Pure metabolites serum spiking protocol ..... 61
**4.3 Result and Discussion** ..... 61
Bibliography ..... 70
5. Conclusions ..... 73
Appendix A: supplementary materials ..... 75

# Abstract

Surface Enhanced Raman spectroscopy (SERS) is a powerful analytical technique that combines high sensitivity and chemical species recognition; specifically, these features are provided by the surface signal enhancement and the vibrational fingerprinting of the Raman spectroscopy, respectively. Thus, the inelastic scattering of the light (or Raman scattering) is used to capture so-called Raman active vibrations in presence of an external source of light. On the base of this phenomenon, unique molecular vibrations determine the identification with high selectivity of a tremendous number of chemical structures. But Raman scattering is by itself a rare event, that occurs only when certain circumstances are achieved. In SERS spectroscopy coherent oscillating of conductive electrons on the metal surface are used to amplify the vibrational energy by the production of a very strong and confined electromagnetic field at the nanoscale. Thus, the outcome signal can be amplified up to ten orders of magnitude compared to the simple Raman effect. Additionally, we refer to SERS plasmonic amplification as localized surface plasmon resonance (LSPR), which allows to reach even a molecular resolution, in presence of specific metal nanostructured surfaces. SERS is also a fast, user-friendly technique, in which these features coupled with the last advancement in optics and photonics (bench, potable and palmar Raman instrumentation can be bought nowadays) have created a fertile field for the spreading of SERS applications. Nevertheless, plasmonic surfaces, or more properly SERS substrates, can be obtained with simple procedures, among the other by coating silver nanoparticles on the paper, obtained with salts reduction in water. Eventually, SERS spectroscopy is a non-destructive technique allowing measurements in aqueous media. For all these features SERS has been introduced, as a promising tool in precision medicine and biofluid analysis. In this frame, the aim of thesis is to develop simple and inexpensive methods to extract biochemical information from complex biological matrixes. The simplest way to do SERS biosensing is to use the Label-free SERS approach. Thus, it is possible, accordingly to the sample compositions and affinity for the metal surface, to identify small molecules and more specifically metabolites. This provides a snapshot of a pool of metabolites whose variation of concentration can be used to extract information on the state of illness of patients. For instance, several label-free SERS studies have reached

promising results in monitoring the therapeutic window or in the classification of patients' state of illness. This is usually reached assessing the differences in the relative concentration of small metabolites. In this frame, I have developed for my PhD project a protocol to extract biochemical information from stool samples. for the first time it has been adopted to study stool samples from celiac patient (celiac disease can be defined as an uncontrolled immunogenic response to the gluten ingestion), with promising results in assessing the compliance of gluten-free diet patients. Eventually, we have developed a fast SERS sampling protocol for human serum using a paper strip that allows to achieve reproducible SERS spectra via centrifugation of few µl of samples spotted on the paper in the presence of silver colloidal nanoparticles. Thus, it was possible to obtain a fast and reliable SERS protocol to be adopted for sampling and biosensing of serum specimen.

# 1. Rationale and background

Nowadays in Biomedicine there is a high demand for new analytical techniques that are more suitable to reach patients' bedside. This can be achieved by the instrumentation miniaturization, and or by more "skinny" analytical procedures: requiring less complex sample treatment, and portable instrumentation. In biomedicine in fact, biosensing standard analytical techniques are tremendously expensive and time-consuming, requiring extensive sample processing or heavy laboratory equipment to provide highly sensitive and specificity.

Specifically, analytical standard techniques for biofluid analysis include liquid and gas chromatography [1], mass spectrometry, fluorescence spectroscopy, and techniques based on specific recognition events such as enzyme-linked immunosorbent assay (ELISA), fluorescence immunoassay (FIA), or radioimmunoassay (RIA) [2]. Among the aforementioned techniques, we can distinguish between mono-marker and univariate-based approach and multiplexing approach. Generally, chromatographic techniques are highly specific and are used to identify a single compound and are more suitable for a quantification of a well define target [1]. On the contrary, MS and NMR techniques are wide range techniques and suitable for multiplexing analysis.

In this fashion, a metabolomic approach becomes possible, and nowadays can be considered an appealing approach, for two main features: firstly, due to its multiplexing and screening capability, that has shown to provide an enormous amount of data at the same time [3]. Secondly, in this frame data analysis can be evaluate by using multivariate data analysis, can be used to assess not only the general state of health of the individuals but to discriminate among different pathologies and the severeness of the illness course; or in other words with prognostic and diagnostic aims [4].

A multiplexing and multi-markers approach is much more valuable, if samples obtained from rutinary analysis can be used to obtain information to replace invasive procedures, such as organ biopsy. But unfortunately, this field is still poorly explored with regard to metabolomics. In fact, just few applications are available and with clinically relevant implication, and none of them can be considered a metabolomics

approach. Specifically, only circulating tumour cells (CTC) and circulating tumour DNA (ctDNA) are in clinical practice and imply immunochemistry and molecular biology techniques, with high specificity, but in which multiplexing capability is still limited to very few cases [5]. Moreover, these techniques remain, in many cases, limited by the incompatibility with the different biofluids, data acquisition time, needing of extremely high expertise level and costs.

Surface enhanced Raman Spectroscopy SERS is a fast analytical technique, in which Plasmonic metal surfaces are used to rise the Raman vibrational signal, defining a powerful surface analytical technique. [2] The Raman spectroscopy provides a chemical fingerprinting of molecules allowing high chemical species recognition, while metal nanostructured surfaces determine an amplification of signal strong enough to candidate SERS for biochemical application and precision medicine. Label free SERS, in which biofluid are presented as is to the plasmonic surfaces, determining a multiplexing metabolic profiling of metabolites that freely absorbs on them [6]. In SERS spectroscopy multivariate data analysis can be used to discriminate metabolites variability that in theory can be used also in liquid biopsy via common biofluid analysis like plasma or serum. Finally, the low cost SERS substrates and relative inexpensive instrumentation can be found, underling as the SERS spectroscopy is a reliable bioanalytical tool.

In this frame, the general aim of the thesis has been to study specific biological matrixes, mainly biofluids, to be analysed by SERS with a direct and label-free approach. The idea behind our investigations is to extract useful biochemical information from those biological matrixes that have shown a composition reflecting some specific physiological and pathological changes, involving the variation or the impairment of the normal metabolism. SERS spectroscopy has been applied successfully for these purposes, showing to be able to explore this biochemical variation under stringent experimental conditions. Since the advantages of SERS spectroscopy are several if compared with some standard bioanalytical techniques, it is reasonable to invest in its applications: SERS is a user-friendly, portable, fast, and inexpensive technique. All these features, readily depict SERS as a potential source of POC (point-of-care) biomedical applications. In more detailed fashion, one among several cutting-edge biomedical applications of SERS is the fast direct biofluids analysis to overcame invasive solid biopsies, in a so-called liquid biopsy mode. But, to complete the picture, we must look

in a more detailed way at the SERS peculiar theoretical and experimental features, bearing in mind that the reliability of label-free SERS applications depends on many fundamental aspects. **I.** In SERS spectroscopy the interaction with plasmonic nanostructures determines the Raman vibrational fingerprint (in other words, the ability to identify chemical species). Thus, the signal depends on specimen chemical affinity for the metal surface. **II.** In this frame, to provide effective SERS substrates must be considered their plasmonic properties, in terms of number and typologies of hot-spots (directly impacting on the signal enhancement), other to the physical properties of the surface. For instance, a solid flat substrate made of gold is less suitable for wet samples than a system with a porous matrix, like paper. **III.** In biofluid Label-free SERS applications we must consider the complex interaction that occurs between biofluids components and the plasmonic metal nanostructures, in which a very specific Nano-bio interface is determined by the biochemical environment and the chemical composition. **IV.** Evaluate the biochemical source of the SERS signal of a biological matrix is an arduous task. Each component must be evaluated with an experimental setup matching as much as possible the biological matrix composition. This can be a very tricky aspect to be tackled, since in general no standard spectra exist for each specific label-free SERS applications. Thus, the identification of specific components must be done by home-made SERS library of metabolites, obtained with the same substrate and protocol. **V.** Finally, the intra and inter-variability of biological samples play a fundamental role in SERS systems, since even a slight change in the chemical composition of the sample (especially for a biological matrix that can be considered synonym of complexity) may directly change the resulting SERS spectra. All these aspects help us to describe the complexity of label-free SERS biosensing, in which high-expertise level is required to explore and optimize each of these steps. Thus, only at the end of this process we can provide solid bases for a biomedical study, in which further classification and regression models should be applied to validate the emerging biochemical difference for a certain issue. At this regard, in this thesis dissertation we focused mainly on the former aspects. Specifically, we have applied a label-free SERS approach with nanoparticles-based substrates on different biofluids. The advantages of this methodology reside in fast and simple substrates preparation. Hence, it was adopted to analyse for the first-time “novel SERS” biofluids like crevicular gingival fluid (CGF) or faecal water (FW), or to simplify existing protocol for more “conventional” bioanalytical matrixes, like human plasma or

serum. Furthermore, many of this bioanalytical target has been used to address very specific biomedical applications in order to correlate the SERS “metabolic profile” with pathological conditions.

## Bibliography


1 Nováková, L. Challenges in the Development of Bioanalytical Liquid Chromatography–Mass Spectrometry Method with Emphasis on Fast Analysis. *Journal of Chromatography A* **2013**, *1292*, 25–37. https://doi.org/10.1016/j.chroma.2012.08.087.

2 Alvarez-Puebla, R. A.; Liz-Marzán, L. M. SERS-Based Diagnosis and Biodetection. *Small* **2010**, *6* (5), 604–610. https://doi.org/10.1002/smll.200901820.

3 Clish, C. B. Metabolomics: An Emerging but Powerful Tool for Precision Medicine. *Cold Spring Harb Mol Case Stud* **2015**, *1* (1), a000588. https://doi.org/10.1101/mcs.a000588.

4 Worley, B.; Powers, R. Multivariate Analysis in Metabolomics. *CMB* **2012**, *1* (1), 92–107. https://doi.org/10.2174/2213235X11301010092.

5 Alix-Panabières, C.; Pantel, K. Liquid Biopsy: From Discovery to Clinical Application. *Cancer Discovery* **2021**, *11* (4), 858–873. https://doi.org/10.1158/2159-8290.CD-20-1311.

6 Bonifacio, A.; Cervo, S.; Sergo, V. Label-Free Surface-Enhanced Raman Spectroscopy of Biofluids: Fundamental Aspects and Diagnostic Applications. *Anal Bioanal Chem* **2015**, *407* (27), 8265–8277. https://doi.org/10.1007/s00216-015-8697-z.

# 2. Raman and SERS spectroscopy

## 2.1. Raman spectroscopy

Raman spectroscopy is a vibrational spectroscopy, in which the Raman or inelastic scattering of the light is used to obtain chemical information, by using a Laser source. In this section will be briefly introduced: the discovery of Raman scattering, basic theoretical aspects on vibrational spectroscopy and Raman scattering, and main concepts of Raman selection rules.

Discovery of Raman scattering

At the end of the XIX century only elastic scattering was supposed to exist, in which the scattered light does not change its energy interacting with the matter. But, in the first quarter of XX century the theoretical calculations had postulated the inelastic behaviour of the light, by the work of Smekel in1923 in [1] that was later confirmed experimentally by the Indian physicist, C. V. Raman [2]. He won the Nobel prize in 1930 for this founding. Raman was able to demonstrate the inelastic scattering behaviour by collecting and focusing the sunlight with a telescope on a pure water sample, either in vapour and liquid state, and a second lens to collect the scattered radiation. Specifically, a filter system with a different wavelength cut-off was placed in-between the focused incident light and the sample and after second lens. Thus, the inelastic scattered light with a wavelength different from the incident one has been collected for the first time.

The Raman scattering

We must introduce the general mechanics of the scattering process: At the beginning the incident light interacts with the matter with no electronic transition, but only distorting the electron clouds, and secondly, a fast relaxation of this energy and a concomitant reirradiation of the light occurs, as light scattering. This process can be defined as elastic scattering since no significant exchange of energy has been involved. On the contrary, if at the same time molecular vibration is involved, as nuclei motions, an exchange of energy can occur between the molecule and the incident light and vice-versa. Hence, the exchanged energy will match one quantum of the vibrational energy of the molecule, defining so an inelastic scattering process: the Raman scattering.

Interestingly, this phenomenon is totally different form absorption either visible or infrared, in which a quantum of energy is absorbed by the molecules to excite an electronical or vibrational level, respectively. Therefore, an absorption process will be allowed only when the energy is equal to the one of an electronic or vibrational transition, instead in scattering process must not. This can be explained looking at entire scattering phenomenon. In presence of the incident light an electronic clouds distortion (polarization) is produced determining an excitation state, which is referred to as *virtual state*, in which a different, fast and real electronic reallocation occurs. Specifically, the energy of this virtual state is proportional to the frequency of the incident light. in Figure 1.1 are reported different initial vibrational states and the possible events occurring when the virtual state is generated. Thus, we have three possible behaviours: i. molecule does not exchange energy with the light, in the elastic process that is termed as Rayleigh scattering (green arrow and peak); ii. Stokes shift (red arrow and peak), in which the starting point is the ground vibrational energy, and relaxation occurs on the first vibrational level; iii. Anti-Stokes shift, (cyan arrow and peak) to the opposite of the stokes shift, ground state is reached after relaxation and reirradiation of the scattered light, but with + Δν(1-0) energy of the initial one. Stokes and Anti-Stokes shifts equally represent the Raman scattering process and are dependent form the population of vibrational levels. This can be easily assessed by looking at the Boltzmann equation (Eq.1).

$$\frac{N_n}{N_m} = \frac{g_n}{g_m} exp\left[\frac{-(E_n - E_m)}{kT}\right] \qquad \textbf{eq.1}$$

In which the population of different $N_m$ and $N_m$ quantic levels is proportional to ΔE ($E_n$ - $E_m$) and to the temperature T (while k is the Boltzmann's constant and g is the grade of degeneracy).

Therefore, in Raman spectroscopy applications the Stokes shifts are generally used, due to the higher population of the ground vibrational level at room temperature. In this process two photon are involved and the virtual state determines the possibility to have a scattering process, thus is not necessary to have energy equal to that of specific quantum level.

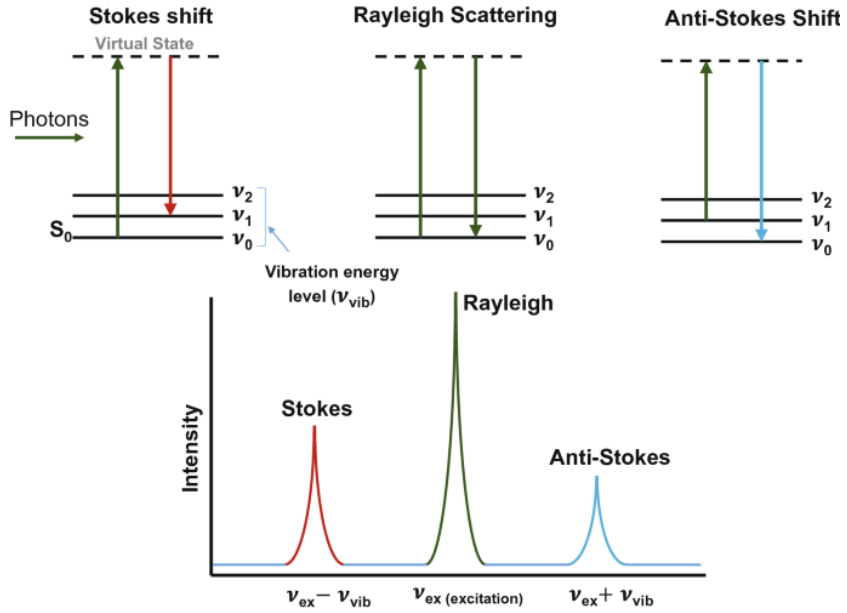


***Figure 1.1*** Possible behaviour of scattered light in relation to the initial vibrational state of specimen molecules, reprinted from [4].

Moreover, considering the intensity of the scattering process reported in figure1.1 (bottom panel), Raman process shows to have an intrinsic low quantum efficiency, which is related to the concomitancy of the excitation induced by the incoming light and a vibrational event. Thus, only one photon is inelastically scattered over $10^6$-$10^8$ incident photons [Long, D. A.]. Only with LASERs introduction and advancement in Photonic field has been possible the spreading of Raman spectroscopy as analytical technique by rising the scattering efficiency, or in other words, introducing brighter sources of light. Moreover, to have an overall comprehension of Raman spectroscopy, molecular vibrations, Raman scattering, and their relationship will be introduced in the following paragraphs.

Molecular vibrations

We can refer to the molecular energy in terms of bonds either orbital and electronic transitions, but we can refer also to the energy related to the molecular motions in space. Thus, excluding the electronic energy, we can define the remaining energy by the degrees of freedom describing all the possible sets of movement in the three dimensions (x, y, z). Hence, three of degrees of freedom are used to describe the translation movements and three are used to describe rotational ones; this is commonly true unless for linear molecules having two degrees of freedom of rotations. Thus, we can consider vibrations as all the displacement allowed in a molecule, by looking at the

degree of freedom across an equilibrium position. We can define them also, as linear combination referring to so called “normal” modes of vibration that account for a unique type of vibration in a molecule. Therefore, the number of vibrations will depend on the degree of freedom and the number of atoms composing it. Thus, we can easily introduce a general rule: molecules with N number of atoms vibrate with 3N-6 normal vibrational modes, excepting for linear one having only 3N-5, by subtracting rotational and translational degree of freedom (for linear molecules the rotation across the bond axes cannot be accounted, leaving the atoms position unchanged). For instance, a diatomic molecule such as $0_2$ has only one vibrational normal mode the symmetric stretch, instead a $C0_2$ molecule will have three normal modes of vibration: symmetrical and asymmetrical stretch and bending. Moreover, with higher number of atoms we can define other typologies of normal modes of vibration, for instances molecules with four atoms, can produce different normal modes of bending, like scissoring or twisting. Balls and sticks representation can be used to show molecular vibrations, as for the typical molecular vibrations reported in **Figure 2.2**. Polyatomic molecules have different normal modes that contribute simultaneously to the vibration of distinct parts of the molecule. Specifically, in complex molecules is difficult to describe all the normal modes of vibration and the overall vibrational state of the molecule. Hence, to identify them properly, geometric principles like group theory are applied, by defining point (or normal coordinates) sharing common symmetry operations. Thus, it is possible to determine when various normal modes contribute to the same vibration [3]. Describe group theory is beyond the scope of this paragraph and a specific dissertation can be found elsewhere [1-3].

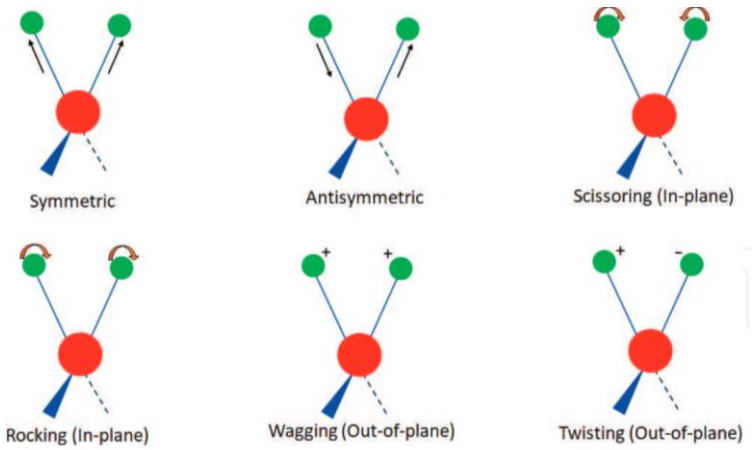


**Figure 2.2** Typical molecular normal modes vibrations, form [X]

Molecular vibrations scattering and polarizability

Normal modes of vibration, as for electronic transition, can be described as multiple states of energy according to the quantum theory, in which at $v_0$ no vibration takes place and at v=1 one quantum of energy is used to have a certain vibrational energy. For sake of simplicity, we can introduce molecular vibrations as energy in function of the internuclear distance, as reported in **Figure1.3** in which we can define both rotational and vibrational levels, other to the electronic ones. As can be argued from the picture, energy profile is related to repulsive and attractive force between nuclei in function of the distance. In this way a morse curve is drawn, which easily describe the energetic behaviour for a single type of vibration [1], where different energy states are allowed according to their quantic energy. In other words, v0 - v1 transition is allowed when a quantum of vibrational energy is absorbed by the molecule.

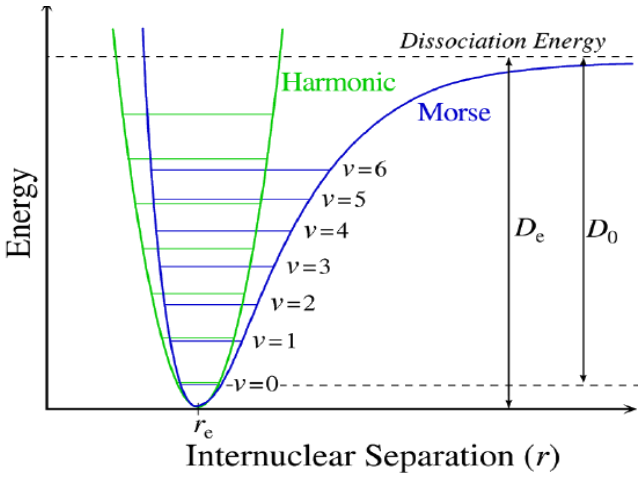


**Figure 2.3** comparison between Morse and harmonic approximation models of vibronic energy in function of atomic distance for a diatomic molecule

In Raman scattering in presence of a virtual excitation state more commonly vibrational energy is expressed as harmonic approximation, in which molecules are represented as masses connected by a spring, according to the Hook's law (eq.1.2). Thus, we can express vibrational energy, as frequency of the vibration, in relation to the atom masses and bond strength of molecules involved in the vibration [1].

$$\nu = \frac{1}{2\pi c}\sqrt[2]{\frac{K}{\mu}} \qquad \text{eq. 1.2}$$

$$E_n = h\left(n + \frac{1}{2}\right)\nu = h\left(n + \frac{1}{2}\right)\frac{1}{2\pi}\sqrt[2]{\frac{K}{m}} \qquad \text{eq. 1.3}$$

Where c is the light velocity, K is the force constant of the bond for a diatomic molecule and $\mu$ is the reduced mass of the related atoms. In this way molecules having lower mass vibrate with higher frequency, as for C-H which vibration lies just above 3000 $cm^{-1}$, instead C-I vibration lies below 500 $cm^{-1}$. At the same extent, we can also define the quantum energy of a generic vibrational n level for a quantum harmonic oscillator as reported in eq. 1.3, in which h is the plank constant and the radical term is derived as the same way form the hook's low and is related to the potential energy. Moreover, in Raman scattering fundamental transition of ±1ν are more likely obtained, thus we can simplify eq. 1.3 as E=h ν.

Eventually, to better clarify what happen when Raman scattering is produced and how to unitary treat molecular vibrations and their interactions with the incident light a brief mathematical demonstration will be introduced.

Conceptually Raman scattering comes out as consequence of the ability of the light to polarize the electron cloud which interact with. We can express the incident light according to the classical electromagnetic theory as an oscillating electrical field producing a radiation oscillating with the same frequency. Thus, we can consider it as induced dipole $\mu_{ind}$, and describe it by the 1.3 equation:

$$\mu_{ind} = \alpha E \qquad \text{eq 1.3}$$

Where α is the Polarizability tensor or the ability to polarize the molecules and E is the electromagnetic field coming from the incident light. The polarizability of an electron clouds is an anisotropic phenomenon, thus it needs to be defined in the three

dimensions by following cartesian axes and becoming a second rank tensor, as in the matrix reported in eq. 1.4.

$$\alpha = \begin{matrix} \alpha_{xx} & \alpha_{xy} & \alpha_{xz} \\ \alpha_{yx} & \alpha_{yy} & \alpha_{yz} \\ \alpha_{zx} & \alpha_{xy} & \alpha_{zz} \end{matrix} \quad \text{eq...1.4}$$

Hence, having the polarizability as tensor makes possible to express it in function of the normal coordinates of the vibrational normal modes of molecules that defines the intensity of the induced dipole over that component. To express this relation properly a Taylor Series will be introduced in the eq. 1.5, describing the interaction between a molecular system and the harmonically oscillating field.

$$\alpha_{ij} = \underline{(\alpha_{ij})_0 + \sum_k \left(\frac{\partial \alpha_{ij}}{\partial Q_k}\right)_0 Q_k} + \frac{1}{2}\sum_{k,l}\left(\frac{\partial {\alpha_{ij}}^2}{\partial Q_k \partial Q_l}\right)_0 Q_k Q_l + \ldots\ldots \quad \text{eq. 1.5}$$

Where $\alpha_{ij0}$ is the $\alpha_{ij}$ value at equilibrium, $Q_k$ and $Q_l$ are normal coordinates for vibrations at frequencies $\omega_k$ $\omega_l$. Terms higher of the second power of Q have been neglected (for simplicity we focus on a singular vibration), thus we may consider only the first term of the series (underlined in yellow), by making a harmonic approximation. Therefore, for a harmonic oscillation the equation 1.6 describe nuclear motion over the time for the same single normal modes $Q_k$:

$$Q_k = Q_{k_0} \cos(\omega_k t + \delta_k) \qquad \text{eq 1.6}$$

Then we can write the expression for the α tensor that result from the k-th vibration as in eq. 1.7

$$\alpha_k = \alpha_0 + \left(\frac{\partial \alpha_{ij}}{\partial Q_k}\right)_0 Q_{k_0} \cos(\omega_k t + \delta_k) \quad \text{eq 1.7}$$

At this point we can substitute equation 1.7 in the induced dipole momentum equation 1.3, that is provided as equation 1.8, for an incident frequency of $\omega_0$.

$$\mu_{ind} = \alpha_k E_0 \cos\omega_0 t = \alpha_0 E_0 \cos\omega_0 t$$

$$+ \left(\frac{\partial \alpha_k}{\partial Q_k}\right)_0 E_0 Q_{k_0} \cos\omega_0 t \cos(\omega_k t + \delta_k) t =$$

$$\alpha_0 E_0 \cos\omega_0 t + \frac{1}{2}\left(\frac{\partial \alpha_k}{\partial Q_k}\right)_0 E_0 Q_{k_0} \cos(\omega_0 t + \omega_k t + \delta_k) +$$

$$\frac{1}{2}\left(\frac{\partial \alpha_k}{\partial Q_k}\right) E_0 Q_{k_0} \cos(\omega_0 t - \omega_k t + \delta_k) \quad \text{eq 1.8}$$

In equation 1.8 we have the scattering effect due to a change in polarizability of a unique normal mode of vibration, that is scattered with $\omega_0 + |\omega_k|$ frequency under the modulation of external electromagnetic field. As can be noticed, it is composed by three terms that account for the behaviour of the scattered light []. In accordance with the explanation previously reported, for the figure 1.3, the first term is related to Rayleigh scattering (green) and the two others are related to the anti-stocks and stokes scattering, respectively (cyan and red). This equations account for the classical electromagnetic theory, but a quantum mechanics theory can be considered to explain the Raman effect, in which the interaction between the excitation light and vibrational and rotational anergy of molecules are bond by the energy transferred form an to quantized and discrete energy levels. Thus, we have to introduce waves equation considering the initial and final state for each normal coordinate, in which we have absorption of emission of energy. In this way we can consider the transitional moment $M_{fi}$ form the initial and final state of the molecule that is expressed by the Eq. 1.9.

$$M_{fi} = \langle \Psi_f \mid \mu \mid \Psi_i \rangle \quad \text{eq 1.9}$$

This equation expresses in Dirac bracket notation the transitional moment for the wave equations $\Psi_f$ and $\Psi_i$ for the initial and final state of molecule in which the induced dipole can be thought in function of the polarizability and the incident field, produced by a $\omega_0$ incident radiation, as for the classical theory. Eventually, we can consider this molecular state in relation to the polarizability, as reported in Eq 1.10, and more specifically we can focus on an element of the $\alpha_{xy}$ of the polarizability, considering only the vibrational part, as shown in Eq 1.11, in which Φ is vibrational wave function.

$$\mu_{fi} = \langle \Psi_f \mid \alpha \mid \Psi_i \rangle \cdot E \quad \text{eq 1.10}$$

$$[\alpha_{xy}]_{fi} = \langle \Phi_f \mid \alpha_{xy} \mid \Phi_i \rangle \quad \text{eq 1.11}$$

By considering the equation 1.7 for a $Q_k$ normal mode of vibration (for a harmonic oscillator model) and Eq. 1.11 shown above, we can conclude that the total vibrational function is the product of the harmonic oscillator wave functions for each of the normal modes, as reported in Eq. 1.12

$$\Phi_i = \prod_k \Phi_{v_{ik}}(Q_k) \quad \text{eq 1.12}$$

Where $\Phi_{v_{ik}}(Q_k)$ is the wave function of the $Q_k$ normal coordinate of vibration that can be expressed in relation to the vibrational quantum number $v_k^i$, that can be in certain state. For instance, if initial and final vibrational quantum number are equal, no Raman effect is achieved, since no change in polarizability has been observed. This result can be easily related to 0 order term, which describe the Rayleigh scattering. For higher terms solution are not so obvious, but the general meaning is vibrational quantum number must change over initial-final state transition to have a change in polarizability for a specific normal coordinate [1]. For the 0-order term the classical theory and the quantum mechanics have the same result, but for higher term the solutions are divergent. As consequences of the harmonic oscillator wave function properties, when we consider the first order term, in $v_f$-$v_i$ transition, for two components j and k with $j \neq k$, transition for j can be equal to 0, instead for k-th element $v_{fk} = v_{ik} \pm 1 v_{kf} = v_{ki} \pm 1$. This corresponds to Raman active vibrations that are more likely fundamental vibrations (overtone $\Delta v \neq 1$ cannot be obtained), in which vibrational quantum number variates of 1 unit. Thus, +1 variation are related to stokes Raman vibration while -1 are related to anti-stock Raman active vibrations. Finally, to have a Raman active vibration is indispensable that at least one element of the α tensor must be different from zero. [3]

The concept of selection rules

Selection rules describe if a vibration is Raman active or not, on the base of the change of polarizability in presence of incident radiation, on the base of the geometrical properties of molecules, that are determined by the group theory, establishing the symmetry element. It is possible to describe if normal modes of vibration are Raman active for simple molecules, by simply looking at the spatial distribution of atoms and the polarizability along a normal mode direction Q [1,3].

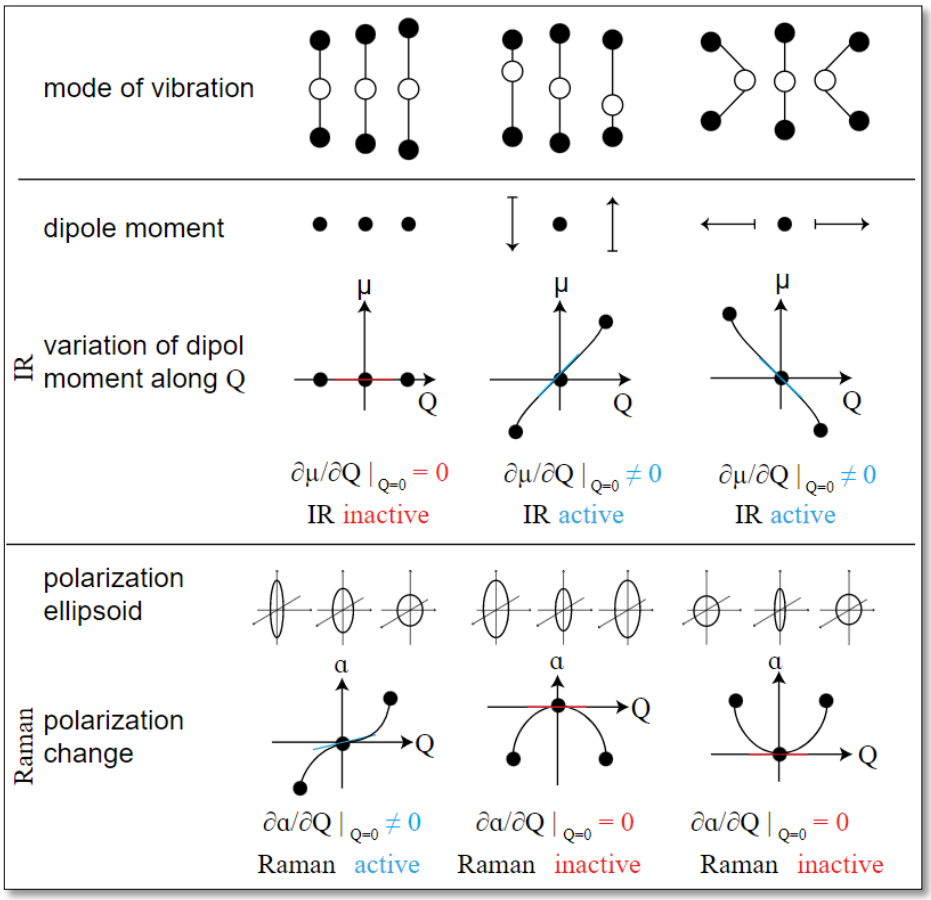


**Figure 1.4** Infrared and Raman normal active mode of vibrations for changing of polarizability and induced dipole intensity along a Q normal coordinate [1]

As reported in the **Figure 1.4**, the symmetric stretch changes the polarizability determining a Raman active vibration; on the other hand, in the asymmetric stretch and bending the polarizability does not change, determining inactive Raman modes. A basic concept can be inferred by looking at the vibrational modes reported in **Figure 1.4**, infrared and Raman mode are mutually exclusive, since a change in polarizability cannot occur simultaneously with a change of induced dipole. For a polyatomic molecules (even to reach macromolecules) group theory is essential to understand the behaviour of the polarizability for specific normal modes, in which distal part of the molecules can influence the polarizability along a single component of the α tensor. A more detailed dissertation of the selection rules is beyond the aim of thesis and has been internally not included.

## 2.2 Surface Enhanced Raman Spectroscopy

SERS spectroscopy is analytical technique that counts on specificity of the vibrational fingerprint of the Raman scattering, and account on metal nanostructured surface to amplify the Raman signal. In presence of the so-called localized surface plasmon resonance (LSPR) a strong local electromagnetic field is generated amplifying the Raman signal. Thus, in principle with SERS it is possible to boost the Raman signal intensity up to $10^8$ times [4]. The dramatic enhancement of the signal has spread the fields of applications of this spectroscopic technique, ranging from analytical chemistry and solid-state physics up to biology and precision medicine [5-7].

In this section will be introduced the SERS historical and theoretical background and the concept of Label Free SERS.

Historical background and general principles

The amplified Raman signal produced by a metal surface was observed by chance in an electrochemical experiment by Fleishman and colleagues in 1973. The enhanced Raman spectra of the pyridine have been observed on the roughened surface of a silver electrode, after the analyte absorption on the surface [5]. Hence at the first time, the high degree of signal intensity was explained by the high absorption rate due to the roughness of the silver surface, without postulating any enhancement effect.

Several years and studies have been spent to demonstrate which were the base mechanisms responsible for the enhancement process. Nowadays, even some aspects are still under debate, two main theories have been developed independently, around 1977 to explain the SERS effect. The first one is commonly referred to as “electromagnetic mechanism” and was proven by Jeanmarie and Van Duyne. specifically, the enhancement effect is due to a rise of the local electromagnetic field, in orthogonal direction to the surface that is under the incident light. In this way molecules that are absorbed on the surface experienced a much stronger electric field than ones far from the surface [8,9]. The higher electromagnetic field is responsible for an increase of the polarizability of molecules absorbed on the surface, that is due to the proportionality between the Raman signal and magnitude of the electromagnetic field.

The latter theory has been proposed by Albright and Creighton [5-10]. In which a part of the enhancement is due to the chemical interaction between the metal surface and the

specimen molecules, for this reason is referred to the “chemical theory”. Furthermore, to produce this kind of the enhancement, the chemical spices need to be chemisorbed on the metal surface, and specifically the effect is due to a charge transfer mechanism. Specifically, it is stronger in presence of molecules with lone electron pairs or with π electrons. Hence, a now molecular species is generated with the absorption and is quite possible to alter vibrational fingerprint of SERS spectra can result rather different form the normal Raman ones. [1-3].

It is supposed that the two mechanisms act synergically, and a strong electromagnetic filed rising from the surface and eventually the chemical modification of the involved molecules determines a change of the selection rules also. This “novel SERS” selection rules depend on the distance form the metal surface, and on the orientation of the molecular moieties in respect of the metal nanostructures, specifically for the z component of the polarizability tensor [3].

More generally, to have a SERS effect molecules absorbed on the metal surface stick together with the metal surface in which surface plasmons are generate by the incident source of radiation and are responsible for the strong local electromagnetic field. Specifically, plasmons are collective oscillations of free conduction electrons that are displaced outside from their shells, by an ω external oscillating frequency due to the laser excitation. According to the material size of the metal surface we can identify *bulk plasmons* which size is bigger than the incident wavelength. On the other hand, *localized surface plasmons* are generated when the size of the incident wavelength is bigger of the metal surface size, as shown in **figure 1.5**. Eventually, when the frequency of the incident light matches LSPs one can be defined a so-called *localized surface plasmon resonance* (LSPR) and is related to a plasmonic absorption phenomena [11]. furthermore, the plasmonic oscillation cannot exist if an external source is not provided, or in other word LSPs do not long-last in the absence of the incident light. Interestingly, LPSR, due to the size too, depends on the optical properties of the metal and the dielectric surface surrounding it, like roughness or geometry. These properties can be finely tuned to develop proper metal nanostructured surfaces to confine LSPRs for specific needing, like high resolution and reproducibility for SERS or plasmonic sensors. Specifically, structure-SPR relation calculations are introduced to define the correct

behaviour of the plasmonic surface also for highly complex metal nanostructures. [12, 13]

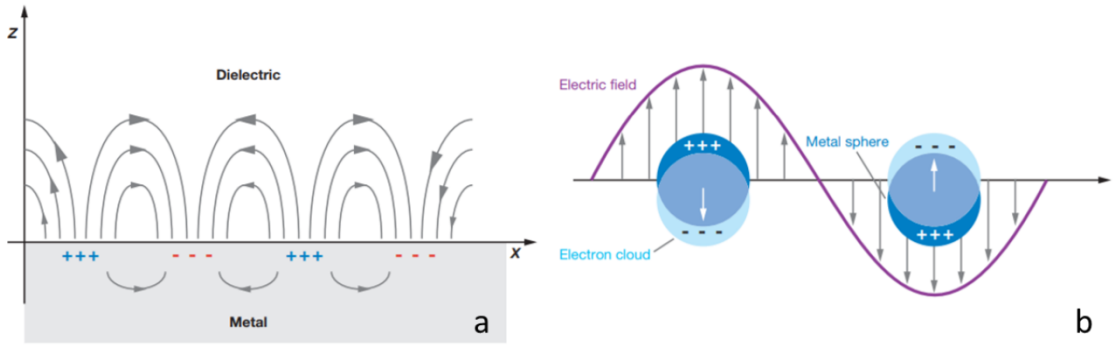


***Figure 2.5*** surface plasmons schemes: a) bulk and b) localized phenomena [12]

Only specific metals are suitable for IR and Raman analysis: coinage metal like gold, silver and copper manly present this specific characteristic, to present and generate the proper plasmonic surface. They also have a very broad range in the plasmonic absorption peak and can generate LSPR with many excitations wavelength, and this is related their ability to be not transparent in the UV-infrared range where plasmonic resonance occurs, allowing the implementation for vibrational spectroscopic application. Other metals can be adopted for SERS analysis like palladium, platinum, nickel, cobalt and so on, but they generate a reduce signal enhancement. this metal is less suitable for biological analysis, since they are prone to oxidation, that is also responsible for the reduction of the plasmonic properties. Silver and gold can be defined standard metal for SERS in bio-analytics, thanks to the stability in biological medium, showing a reduced aging and oxidation in comparison to other metals. [3]

Theoretical aspect

In this section will be introduced in a simplified version some theoretical aspects related to the SERS: i) the electromagnetic model of SERS, ii) geometry or aggregation effect (like the hot-spots generation).

i) Electromagnetic model:

This part has been thought to be in accordance with the Mie scattering theory, in which a spherical a metal nanoparticle is considered of radius a, in presence of a source of radiation of light of λ wavelength, and λ >> a, that is the simplest approximation of LSPR system. [17]. In this approximation the magnitude of the electromagnetic field

surrounding the nanoparticles (*Eout*) can be calculated by the Maxwell's classical electromagnetism equations, that is provided in the **eq. 1.13:**

$$E_{out}(x,y,z) = E_{0\hat{z}} - \left(\frac{\varepsilon(\lambda) - \varepsilon m}{\varepsilon(\lambda) + 2\varepsilon m}\right) a^3 E_0 \left(\frac{\hat{z}}{r^3} - \frac{3}{r^5(x\hat{x} + y\hat{y} + z\hat{z})}\right) \quad \text{Eq 1.13}$$

Thus, the Eout depends on the distance from the particle's surface, size and optical properties, and the dielectric properties of the medium, other to the light frequency. More specifically, the bulk properties of the material are related to the dielectric function ε(ω), instead the properties of the dielectric are defined by dielectric constant $\varepsilon_{m,,}$ that describe the behaviour of the material under an external electrical field. This is a complex number that depends on the wavelength and on the structure of the material, and is presented in eq. 1.14:

$$\varepsilon(\lambda) = \varepsilon'(\lambda) + i\varepsilon''(\lambda) \quad \text{Eq 1.14}$$

Where the real part of the equation is related to phase offset form the incident light and the final frequency, while the imaginary part is related to the radiation absorption. Optical properties and macroscopic behaviour are connected by the equation 1.15 that confirm the fact that the metal polarizability can be derived from the dielectric function itself, in the case of a metal sphere in a medium with $\varepsilon_m$ dielectric constant:

$$\alpha = a^3(\varepsilon(\lambda) - \varepsilon m / \varepsilon(\lambda) + 2\varepsilon m) \quad \text{Eq 1.15}$$

In which $\alpha$ is the metal polarizability, $\varepsilon(\lambda)$ is the dielectric function for the nanoparticle. the term in brackets is the same of the equation 1.13 and describes the Enhancement of the external electromagnetic field $E_{out}$,and is related to incident $\lambda$ and to the radius of the nanoparticles.

On the base of eq 1.15 we can have the enhancement of the SERS signal only when the denominator tend to be 0, and when the dielectric function is equal to -2 $\varepsilon_m$ ..Thus, to match this condition we can consider the proper dielectric constant of the medium, buat above all metals that has a dielectric function able to be active with the adopted wavelength. Gold and silver metals can provide a strong electromagnetic for a broad range in the visible and mid-infrared wavelengths, having larger range for the plasmonic resonance frequencies [16].

In SERS we have the exchange of energy between the plasmonic surface and analyte the is involved in the changed of the polarizability. This effect is proportional to the distance and decreases with $10^{th}$ power of the distance from the metal surfaces. We can conclude that this a near field process and is related to the very external layers of the metal surface [12] that are responsible for the field enhancement. It is also possible to introduce the enhancement factor (EF) that is the ratio between the normal Raman intensity and SERS intensity for a specific peak at the surface, and represents the capability of the field metal surface to generate enhancement signal and can be expressed in first approximation by the relation reported in eq 1.16:

$$EF(r,\lambda) = \left|\frac{E_{out}(r,\lambda)}{E_0(r,\lambda)}\right|^4 = \frac{I_{SERS}/N_{surf}}{I_{raman}/N_{vol}} \quad \text{Eq 1.16}$$ **Errore. Il segnalibro non è definito.**

In which r is the distance and $\lambda$ wavelength of the incident light. On the right side of the equation we can found an empirical formula expressing SERS intensity normalized for the absorbed molecules on the enhanced substrate $N_{surf}$, while $I_{Raman}$ represents the Raman intensity normalized for the number of molecules in the excited volume $N_{vol}$

ii) SERS hot spot: geometry and aggregation

LSPR on the plasmonic surface can be finely tuned playing with specific properties like modifying shape and size of surface, as the same extent it possible to rise the SERS intensity response by several orders of magnitude.

In order to have a significant SERS effect, particle size must range from 10 to 100 nm, and we have to match the condition of wavelength higher than the particles radius, otherwise we cannot consider the external electromagnetic field homogenous without confining the field on the single particles. However, if we consider nanoparticles smaller

of 10 nm or of few nm, they are not able to generate a resonant effect and do not contribute to the SERS effect significantly. On the contrary, with bigger particles than 100 nm different plasmonic resonances arise from the particles determining e destructive effect and resulting in a drop of the SERS effect.

Size related effect is also influenced by the shape of the nanostructure used as plasmonic surface, and accordingly to their shape it is possible to obtain an EF for each of them. Furthermore, Exist several shapes for SERS plasmonic surface like cylinder, cones, rods, stars and so on. All these shapes exhibit different properties in relation to the number of their faces, to the direction in relation to external field [15,18 ].

One of the main key points to be consider for the SERS EF is the aggregation effect. One of the most effective SERS enhancer is constituted by a dimer of spherical nanoparticles aggregated that considerable overcome the EF reachable with a single particles, in this condition it is possible to get in principle a single molecule detection [12, 23]. At the same extent, the orientation of the plasmonic surface and the specimen molecules in relation to the external field and to each other, play an important role in EF generation. To generate the strongest plasmonic coupling interparticle axes must be parallel to the oscillation to the external electronic field, instead normal modes determining Raman active vibration orthogonal to the surface are preferentially enhanced. Surprisingly, when the direction is perpendicular to the interparticle axes the EF falls to the level of an isolated particle.

We can identify the centre of aggregation between nanoparticles has a Hot-spot location in which we have the maximum EF, as in the case of the interparticle location. Hot-spot formation can be determined by the confluence of two LSPR on surface with nano-roughness, by coupling [15,20,22].

In conclusion, geometric tailoring of nanoparticles can be used to select a desired LSPR for specific purposes. But the variation of hundreds of many other parameters can be also used to tune the EF for SERS application, demonstrating the almost infinite possibility to crate various and even more effective LSPR structures, other to the complexity of this topic.

## 2.3 SERS and the label-free approach for biosensing

In the frame of a bioassay, whether to go for a labeled or unlabeled substrate depends on the specific application.

In the "omic" era, the amount of information that can be retrieved from a biological sample is overwhelming, but still the challenge is to identify which are the most relevant information in the bunch and multivariate data analysis can give some keys to this end. Genomics, proteomics, microbiomics, lipidomics, transcriptomics, metabolomics are some of the branches that have grown in the last two decades since they led to the rapid discovery of several possible biomarkers for diagnostic and theranostic purposes. To date, all the techniques belonging to these fields are basically devoted to find and characterize biomolecules that are involved in disease-related biochemical pathways, like chromatography-coupled mass spectroscopy, fluorescence spectroscopy, immunoassays tests, but only few of these have turned into realistic applications [38].

The new challenge is to change point of view and to move from the classic "single to few biomarkers" detection to reach the multiscale data, namely from a targeted approach to an untargeted one. The purpose is to consider the whole signal as a fingerprint of the actual situation, as a multi-marker, irrespective to the used technique. SERS substrates fabrication may include, or not, the chemical functionalization of the nanostructure. The labels on the NPs are the key for the detection of specific molecules: the substrate is chemically tailored in order to identify a specific target [18,35,37]. Functionalized multiple arrays are a step forward in the SERS detection of metabolites, but it is still complex to build.

The label-free method, on the contrary, employs NPs without any tag, naked, apart from the shield that works as capping and stabilizing agent: all the molecules present in the specimen can virtually reach the SERS surface, irrespective for their nature, though with different kinetics [21,24,40]; the final spectra would reflect the affinity of the analytes for the metal surface.

Indeed, in the present work the label-free approach has been used, with the specific intent to propose highly versatile SERS substrates, simple in nature and simple to use.

# Bibliography


1. Smith E and Dent G 2004 Modern Raman Spectroscopy - A Practical Approach: Smith/Modern Raman Spectroscopy - A Practical Approach (Chichester, UK: John Wiley & Sons, Ltd)
2. Venables W N and Ripley B D 2002 Modern Applied Statistics with S (New York, USA)
3. Long D. A. The Raman Effect: A Unified Treatment of the Theory of Raman Scattering by Molecules; Wiley: Chichester; New York, 2002.
4. Smith W E 2008 Practical understanding and use of surface enhanced Raman scattering/surface enhanced resonance Raman scattering in chemical and biological analysis Chem. Soc. Rev. 37 955–64
5. Albrecht M G and Creighton J A 1977 Anomalously intense Raman spectra of pyridine at a silver electrode Journal of the American Chemical Society 99 5215– 7
6. Matousek P, Towrie M, Stanley A and Parker A W 1999 Efficient Rejection of Fluorescence from Raman Spectra Using Picosecond Kerr Gating Appl. Spectrosc., AS 53 1485–9
7. Le Ru E C, Blackie E, Meyer M and Etchegoin P G 2007 Surface Enhanced Raman Scattering Enhancement Factors: A Comprehensive Study The Journal of Physical Chemistry C 111 13794–803
8. Campion A and Kambhampati P 1998 Surface-enhanced Raman scattering Chem. Soc. Rev. 27 241–50
9. Fleischmann M, Hendra P J and McQuillan A J 1974 Raman spectra of pyridine adsorbed at a silver electrode Chemical Physics Letters 26 163–6
10. Bantz K C, Meyer A F, Wittenberg N J, Im H, Kurtuluş Ö, Lee S H, Lindquist N C, Oh S-H and Haynes C L 2011 Recent progress in SERS biosensing Physical Chemistry Chemical Physics 13 11551 9
11. Jeanmaire D L and Van Duyne R P 1977 Surface raman spectroelectrochemistry: Part I. Heterocyclic, aromatic, and aliphatic amines adsorbed on the anodized silver electrode Journal of Electroanalytical Chemistry and Interfacial Electrochemistry 84 1–20
12. Ritchie R H 1957 Plasma Losses by Fast Electrons in Thin Films Phys. Rev. 106 874–81 66
13. Willets K A and Van Duyne R P 2007 Localized Surface Plasmon Resonance Spectroscopy and Sensing Annual Review of Physical Chemistry 58 267–97
14. Mayer K M and Hafner J H 2011 Localized Surface Plasmon Resonance Sensors Chemical Reviews 111 3828–57
15. Bonifacio A, Dalla Marta S, Spizzo R, Cervo S, Steffan A, Colombatti A and Sergo V 2014 Surface-enhanced Raman spectroscopy of blood plasma and serum using Ag and Au nanoparticles: a systematic study Anal Bioanal Chem 406 2355–65
16. Schlücker S 2014 Surface-Enhanced Raman Spectroscopy: Concepts and Chemical Applications Angewandte Chemie International Edition 53 4756–95
17. Aroca R 2006 Surface-Enhanced Vibrational Spectroscopy (John Wiley & Sons)
18. Horvath H 2009 Gustav Mie and the scattering and absorption of light by particles: Historic developments and basics Journal of Quantitative Spectroscopy and Radiative Transfer 110 787–99
19. Lane L A, Qian X and Nie S 2015 SERS Nanoparticles in Medicine: From LabelFree Detection to Spectroscopic Tagging Chem. Rev. 115 10489–529

20. Kneipp K, Kneipp H, Kartha V B, Manoharan R, Deinum G, Itzkan I, Dasari R R and Feld M S 1998 Detection and identification of a single DNA base molecule using surface-enhanced Raman scattering (SERS) Physical Review E 57 R6281–4
21. Kneipp K, Kneipp H and Bohr H G 2006 Single-Molecule SERS Spectroscopy Surface-Enhanced Raman Scattering: Physics and Applications Topics in Applied Physics ed K Kneipp, M Moskovits and H Kneipp (Berlin, Heidelberg: Springer Berlin Heidelberg) pp 261–77
22. Moskovits M 1982 Surface selection rules J. Chem. Phys. 77 4408–16
23. Koh A L, Bao K, Khan I, Smith W E, Kothleitner G, Nordlander P, Maier S A and McComb D W 2009 Electron Energy-Loss Spectroscopy (EELS) of Surface Plasmons in Single Silver Nanoparticles and Dimers: Influence of Beam Damage and Mapping of Dark Modes ACS Nano 3 3015–22
24. Stiles P L, Dieringer J A, Shah N C and Van Duyne R P 2008 Surface-Enhanced Raman Spectroscopy Annual Review of Analytical Chemistry 1 601–26
25. Amendola V and Meneghetti M 2009 Laser ablation synthesis in solution and size manipulation of noble metal nanoparticles Phys Chem Chem Phys 11 3805– 21
26. Neddersen J, Chumanov G and Cotton T M 1993 Laser Ablation of Metals: A New Method for Preparing SERS Active Colloids Appl. Spectrosc., AS 47 1959–64
27. Tolaymat T M, El Badawy A M, Genaidy A, Scheckel K G, Luxton T P and Suidan M 2010 An evidence-based environmental perspective of manufactured silver nanoparticle in syntheses and applications: A systematic review and critical appraisal of peer-reviewed scientific papers Science of The Total Environment 408 999–1006
28. Sha M Y, Xu H, Penn S G and Cromer R 2007 SERS nanoparticles: a new optical detection modality for cancer diagnosis Nanomedicine (Lond) 2 725–34
29. Cervo S, Mansutti E, Del Mistro G, Spizzo R, Colombatti A, Steffan A, Sergo V and Bonifacio A 2015 SERS analysis of serum for detection of early and locally advanced breast cancer Anal Bioanal Chem 407 7503–9
30. Alvarez-Puebla R A and Liz-Marzán L M 2010 SERS-Based Diagnosis and Biodetection Small 6 604–10
31. Jaworska A, Fornasaro S, Sergo V and Bonifacio A 2016 Potential of Surface Enhanced Raman Spectroscopy (SERS) in Therapeutic Drug Monitoring (TDM). A Critical Review Biosensors 6 47
32. Gutés A, Carraro C and Maboudian R 2010 Silver Dendrites from Galvanic Displacement on Commercial Aluminum Foil As an Effective SERS Substrate Journal of the American Chemical Society 132 1476–7
33. Luo S-C, Sivashanmugan K, Liao J-D, Yao C-K and Peng H-C 2014 Nanofabricated SERS-active substrates for single-molecule to virus detection in vitro: A review Biosensors and Bioelectronics 61 232–40
34. Polavarapu L and Liz-Marzán L M 2013 Towards low-cost flexible substrates for nanoplasmonic sensing Physical Chemistry Chemical Physics 15 5288
35. Gurian E, Bellich B and Cesàro A 2016 Polysaccharide solutions and gels: Isothermal dehydration study by dynamic calorimetric experiments with DSC Food Hydrocolloids 61 163–71 35 [91] Yu W W and White I M 2013 Inkjet-printed paper-based SERS dipsticks and swabs for trace chemical detection Analyst 138 1020–5
36. Chin C D, Linder V and Sia S K 2012 Commercialization of microfluidic point-ofcare diagnostic devices Lab Chip 12 2118–34

37. Alvarez-Puebla R A and Liz-Marzán L M 2010 SERS-Based Diagnosis and Biodetection Small 6 604–10
38. Hasi W-L-J, Lin X, Lou X-T, Lin S, Yang F, Lin D-Y and Lu Z-W 2015 Chloride ionassisted self-assembly of silver nanoparticles on filter paper as SERS substrate Appl. Phys. A 118 799–807
39. Wang Y, Yan B and Chen L 2013 SERS Tags: Novel Optical Nanoprobes for Bioanalysis Chemical Reviews 113 1391–428
40. Liu R, Xiong Y, Guo Y, Si M and Tang W 2018 Label-free and non-invasive BSSERS detection of liver cancer based on the solid device of silver nanofilm Journal of Raman Spectroscopy 49 1426–34
41. Lane L A, Qian X and Nie S 2015 SERS Nanoparticles in Medicine: From LabelFree Detection to Spectroscopic Tagging Chem. Rev. 115 10489–529
42. Bonifacio A, Cervo S and Sergo V 2015 Label-free surface-enhanced Raman spectroscopy of biofluids: Fundamental aspects and diagnostic applications Analytical and bioanalytical chemistry 407 8265–77

# 3. label free SERS for spectroscopic investigation on stool samples: the case of study of coeliac disease

This chapter is related to published articles that is reported as reference [1], citation of the supplementary section of this reference are reported when not necessary strictly to the dissertation, the reader can find detailed looking directly to supplementary information in the Appendix A.

## 3.1 introduction

label free SERS in is a powerful approach to identify metabolites on the base of the metal affinity as reported in the introduction chapter. This can provide a relative fast and complementary tool for metabolomic analysis in which a *snapshot* of the level of a small number of metabolites can be used to clarify a pathological situation or a physiological impairment. In this frame SERS can be considered a possible alternative to expensive solution, like mass spectroscopy methods. In this sense we can describe SERS as metabolomic techniques, but with specific limitation. Specifically, a metabolomic approach is a system biology approach, whom scope is to identify quantitatively and qualitatively small metabolites.

The target of metabolomic approach in biomedicine are easy-to-obtain and store biofluid like serum, urine and tissues. Stool samples are less used and are generally required for very specific diagnostic purposes. However, stool sample can be obtained in a non-invasive way and can be easily store in -80°C freezers for several months. Problems arise with the complexity of the material, that can be considered a very complex and inhomogeneous biological sample. Faecal composition depends on several biological factors: inner factors such as gut microbiota and nutrition, or external like xenobiotics; all these sources of variability depict this matrix as one of the most variable from a biochemical point of view.

Nowadays the study of faecal composition with an -omics approach is rise in attention due to the linkage with the mesenteric nervous system [2] and psychological health and several pathological conditions, like celiac disease on which is based this preclinical

study presented in this chapter. these outcomes are due to the development of microbiome sequencing and integrated technique for metabolomics analysis of the faecal samples for highly informative study on the interaction between the gut microbiota GM and the host [3].

Gut microbiota is formed all the organisms that are hosted in the gut and can be divided in multiple phyla of archaea, bacteria, and various species of eukaryotic organisms. This integrated net of microbes is devoted to very specific and essential physiological functions, among the others, a very first “immunity” gut response, food and fibres intake, and the regulation of a paracrine response with multiple endocrine functions, for instance in regulating some central nervous responses [3].

An impairment in the GM can alter the metabolism and degenerate in several pathology with a severe state of illness too. Particularly, in many of them, both the microbiota and the gut metabolome are altered, for instance in systemic disorders (like central nervous system), in colorecta cancer [4], in metabolic syndrome [6] and in lupus erythematosus [5]. In all these cases the metabolic profile can provide cues on the real physiological state of the patient, helping to understand the effect in the microbiota profile changing, with the hope to improve prognosis and diagnosis of several diseases. Up to now the main approach to study the gut microbiome is the sequencing of rRNA 16S (ribosomal RNA of 16S subunit) that provide specific and precise taxonomic information on the microbiota composition, via a faecal sample analysis [9]. Ribosomal RNA sequencing is not an error-free process, and samples alteration can reduce the RNA stability. But, more importantly it is a laborious process and general application reserved to small number of samples, as in the case of clinical practice.

For this reason, the gold standard techniques for metabolomic analysis and quantification of faecal samples are the hyphenation of high-resolution mass spectroscopy-based techniques (HRMS) coupled with the high-performance chromatography. With HSMR high resolution and sensitivity in metabolites quantification can be reach, although calibration with standard is still required, and usually require high expertise level users and it tremendously time-consuming. Hence, all these aspects taken together depict HRMS as an expensive analytical technique. Thus, it is arduous to imagine it as rutinary application in clinics, for the most part of healthcare treatments. Up to now, fast and inexpensive techniques for an accurate identification of

faecal metabolites are still missing, especially if are thought for routinary clinical applications that usually are limited by unspecialized personnel and difficulties in samples pre-treatment.

As previously reported in the chapter 2, SERS can produce metabolomic profile from biofluid with high sensitivity up to a single molecule measurement and with a non-destructive samples interaction [10][11]. In this frame, small metabolites interacting with the SERS hot-spots, on the metal surfaces (SERS substrate) can beneficiate of the LSPR effect determining the enhancement of the Raman effect, enabling high sensitivity detection of specimen molecules. SERS analytical session are user friendly, do not requiring any expertise to be performed and finally, spectra can be acquired in few seconds, resulting in a very fast analytical technique.

In SERS sample preparation is usually minimal, above all for label free SERS applications, in which molecules of the samples (e.g., a human biofluid) are left free to absorb on the metal substrate. Thus, two factors are pivotal in SERS applications: the relative concentration of the species in the biological matrix and the affinity for the metal surface, which is the most important one, since the SERS effect strongly depend on the distance as reported in detailed in the chapter 2. The metal surface act as selective filter determining which kind of molecules can be observed in the SERS spectra. This provide a “biochemical snapshot” for a pool of metabolites that can be used to evaluate a specific pathological condition, or in other word, to provide possible relevant clinical information with a very reduced effort in the operative part. Label-free SERS can be useful in situation in which no or little information about the metabolite composition under study is known.

Hence, the aim of this chapter has been to develop a fast and sensitive SERS method for human faecal samples analysis, providing reliable SERS spectra of the metabolic components, and moreover to characterize the signal in terms of useful information that can be achieved in this specific matrix, by also using a simple protocol and a compact and portable Raman instrumentation.

Finally, the developed protocol has been adopted in a case of study on stool samples collected form patient at paediatric age with the coeliac disease (CD) the diagnosis (CD group), or for patients that are already in gluten-free diet (GFD group). This has been the first study in which SERS was used to study faecal samples from coeliac patients. CD

is autoinflammatory and autoimmune disease related to the ingestion of gluten, in which has been recognized a genetic component. After reaching the diagnosis the only possible treatment is to follow a gluten free diet to reduce the autoimmune response. A prolonged ingestion of gluten for coeliac patient can degenerate in reduction of number villus in the gut mucosa, leading to a reduction of nutrient absorption up to gut cancer. Although also others gut uncorrelated pathologies like anaemia, depression, infertility, and osteoporosis can be developed without a stringent GFD. [12]. Evaluate the compliance of patient to the diet is unmet clinical needing that usually is correlated to the presence of symptoms, and a fast test do not exist in alternative to immunoglobulin assay. Finally, recent study has started to correlate CD to gut microbiome and metabolome. Thus, the study of metabolome and metabolites in GFD and CD patient might be useful for further clinical purposes [13-15].

## 3.2 Experimental part

### Reagents

Methanol used to obtain faecal extracts, hypoxanthine, xanthine and bilirubin, and all the chemicals and solventsused in the synthesis of AuNP were purchased from Merck (Merck KGaA, Darmstadt, Germany). E.Z.N.A® StoolDNA kit (Omega Bio-Tek) was used to extract stool DNA. AccuStartII PCR ToughMix 2X (Quanta Bio) plus Eva-Green™ 20X (Biotium) was used in real-time amplification. Mag-Bind®TotalPure NGS (Omega Bio-Tek) was used to purify PCR products. A Qubit dsDNA HS AssayKit (Thermo Fisher Scientific) was used to quantify PCRproducts. Ion PGM™ Template Hi-Q OT2 400 View, IonPGM™ Enrichment Beads and Ion PGM™ Hi-Q™ viewSequencing Kit (Thermo Fisher Scientific) were used for sequencing.

### Faecal samples

**Table 3.1** Number, sex and age distribution of subjects enrolled into the study divated by gripu of patients (controls CTR; coeliac disease CD, gluten-free diet, GFD).

| | F | M | Total | Median age (quartiles) |
|---|---|---|---|---|
| CTR | 3 | 5 | 8 | 7 (5.75–10) |
| CD | 7 | 2 | 9 | 10 (4–14) |
| GFD | 7 | 3 | 10 | 12.5 (12.0–15.5) |
| Total | 17 | 10 | 27 | |

Samples were collected by IRCCS Burlo Garofolo from subjects instructed to collect and keep a sample of stools at − 20 °C. Sample characteristics are reported in Table 3.1 and in Supplementary Fig. S1. Specimens were delivered and kept at − 20 °C until analysis. Once thawed, the samples were homogenized and two aliquots were prepared for SERS and genomic analysis. Written informed consent was obtained from the parents of the children enrolled, and the study was approved by the hospital's independent1 3 ethical committee (CEUR-2019-Os-157). Samples from CD patients were collected at the time of diagnosis, and from patients in GFD from at least 1 year.

SERS measurements

The aqueous colloidal dispersion of gold nanoparticles (AuNP) used as SERS substrates was synthesized according to the method of Turkevich et al. [16], involving the reduction of Au(III) salts with sodium citrate. All solutions were prepared with ultrapure water, MilliQ (Millipore, USA), and all the glassware was cleaned with a Nochromix ® (Godax Laboratories, Inc.) solution (with H2SO4), *aqua regia* (1 HNO3:3 HCl, vol.), and finally thoroughly rinsed with MilliQ water before use. Operatively, 10.6 mg of NaAuCl4 2H2O (sodium tetrachloroaurate dihydrate) was added to 25 mL of water in an Erlenmeyer flask and heated to boiling. Then, 750 µL of sodium citrate tribasic dihydrate aqueous solution (1%, 1 g/100 mL) was rapidly added, and the solution was kept boiling for 20 min under vigorous stirring and reflux using a water-cooled condenser. Ultimately, the colloidal dispersion was left to cool down to room temperature. Nanoparticles were characterized by UV–visible spectroscopy (Cary100, Agilent, Santa Clara, USA) and transmission electron microscopy (EM 208, Philips, Amsterdam), and had an average/median size of 53.6 nm. The UV–visible extinction spectrum, TEM micrograph and size distribution (as calculated from TEM images) figure 3.1.

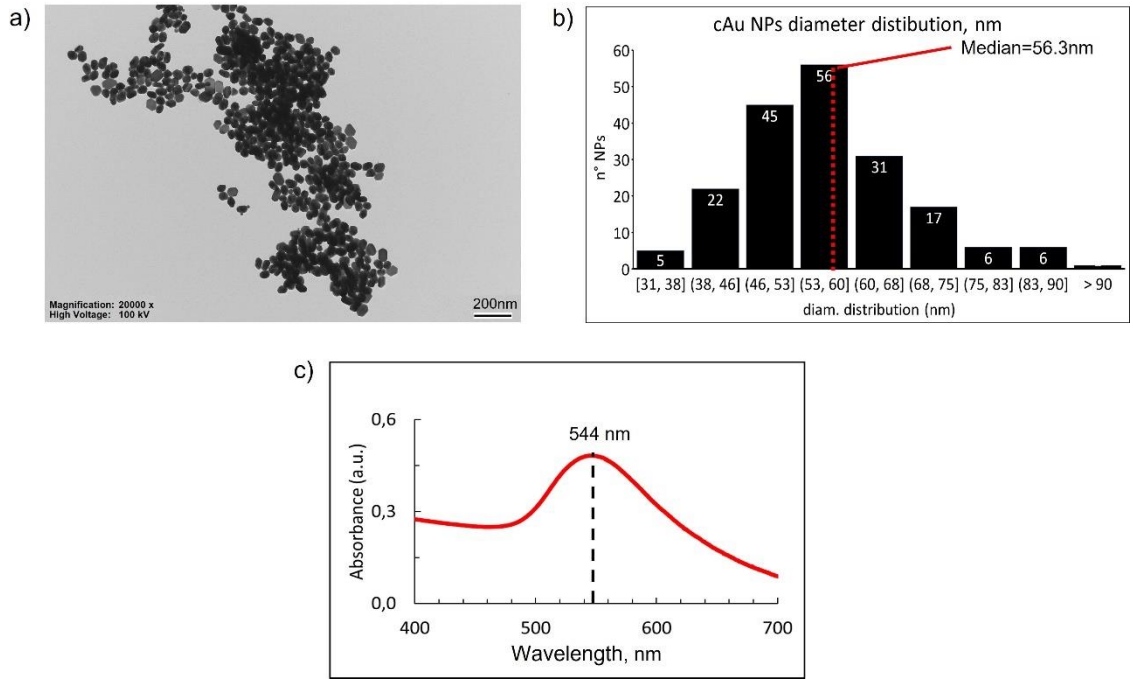


***Figure 3.1*** Characterization of gold colloidal Nanoparticles; a) TEM images of gold NPS ; b) diameter distribution calculated from TEM images; and c) visible spectroscopy of gold nanoparticles plasmonic peak

SERS data pre-processing and analysis

Spectra have been entirely processed using the R environment for data analysis [17]—version 4.1.0 (2021–05-18). In particular, the package hyperSpec [18] was used for data import and visualization. The preprocessing steps included (i) Raman shift range selection (300–1800 cm− 1), (ii) baseline correction (package baseline [19], method "als", lambda parameter = 4) and (iii) vector normalization. Examples of baselines are shown in Fig. S3 of the Supplementary information. Principal component analysis (PCA) was performed using the *prcomp* function, centring but not scaling data. The cumulative proportion of explained variance for the first 19 principal components of the dataset is available as Supplementary information (Fig. S5). The Welch's unequal variances *t* test with correction for false discovery rate for the scores of the first principal component was performed by using the *pairwise.t.test* function (p.adjust.method = "BH", pool.sd = FALSE). Spearman's correlation coefficients between scores of the first principal component and operational taxonomic unit (OTU) relative abundances were computed by using the *cor.test* function, to measure the strength of association between these two variables [20]. For each correlation coefficient, the chance that the correlation is due to chance was estimated by calculating the *p*value (retuned by the *cor.test* function as well). The *p* values obtained were corrected by estimating the false discovery rate

(FDR) by using the *p.adjust* function, according to the Benjamini–Hochberg method [21]. All figures were prepared using the R environment for data analysis [17].

Genomic Analysis

Library preparation and sequencing were performed at the DNA sequencing facility of the Department of Life Sciences of the University of Trieste [22].

Genomic data pre-processing and analysis

The CLC Microbial Genomics Module as a part of the CLC Genomics Workbench 20.0 (QIAGEN Digital Insights, Aarhus, Denmark) was used to analyse alpha and beta diversity, and the composition of the bacterial community [22].Raw sequencing reads were imported into the CLC environment, and subjected to quality control, primer and adapter sequence removal and minimum size cut-off of 150 bp. The OTUs were picked by mapping sequences against the SILVA 16S v132 97% database [24] at the same identity percentage to observe OTU at the species level. Next, the OTUs were aligned using multiple sequence comparison by log-expectation and used to construct a "maximum likelihood phylogenetic tree" followed by alpha and beta diversity analyses. We estimated the effect size and significance on beta diversity for grouping variables with PERMANOVA [25]. PERMANOVA is an acronym for "permutational multivariate analysis of variance", and it is a semi-parametric multivariate statistical test used to compare groups by testing the null hypothesis that the centroids and dispersion of the groups as defined by a distance measure (in our case the Bray–Curtis dissimilarity) are the same for all groups. PERMANOVA applied to our OTU dataset returned pseudo *f*-statistic values [25] and *p* values (Bonferroni corrected) [26, 27]. For a detailed description of the meaning of the pseudo *f*-statistic (or pseudo *f*-ratio), see [25]. Differential abundance analysis [28] was performed by modelling each OTU as a separate generalized linear model (GLM), where it is assumed that abundances follow a negative binomial distribution. The Wald test was used to determine the significance of group pairs.

## 3.3 Result and discussion

SERS spectra can be observed mixing methanol faecal extracts with Au nanoparticle dispersions. (Fig. 1). Extraction with methanol is a consolidated technique in faecal

metabolomics literature [29] and in previous studies normal Raman spectra of faecal samples [30].

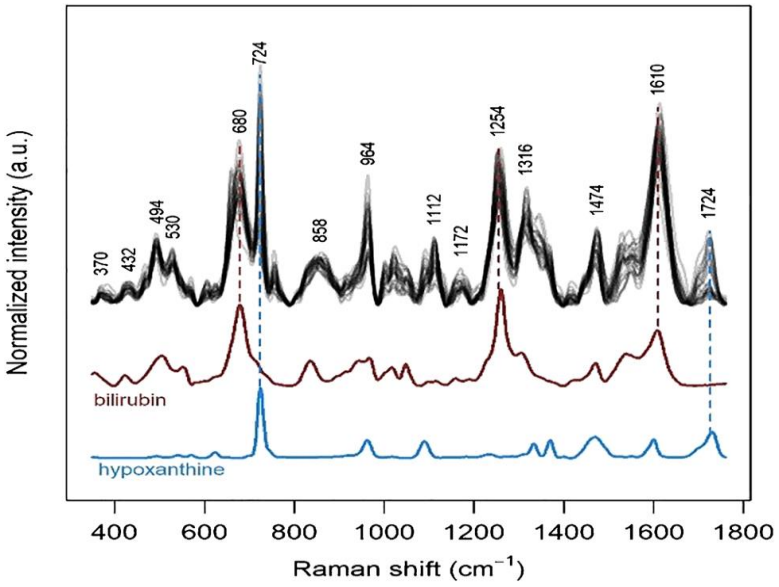


**Figure 3.2** All SERS spectra of dataset (normalized). SERS spectra of bilirubin and hypoxanthine are shown stacked. AuNPs at 785nm excitation wavelength reprinted from [1]

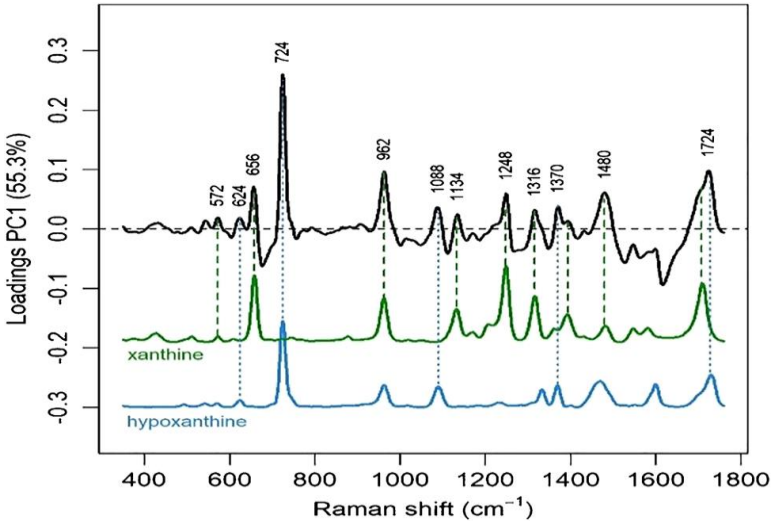


**Figure 3.3** PCA loadings of the first principal component PC1, showing which spectral region are responsible for most part of the variance into the dataset. Below are reported the spectra of xanthine and hypoxanthine respectively in green and light blue. AuNPs at 785 nm of laser excitation

The protocol used in this study has been optimized to enhance SERS spectra repeatability and resulted in the first SERS spectra acquisition from faecal samples. Although a specific comparison between SERS and normal Raman from previous study spectra is problematic, due to an imprecise estimation of the Raman shifts of bands maxima, evident differences between the spectral profiles can be appreciated, without similar bands even though SERS spectra show some variability, many common features can be observed (**Figure. 3.2**), as variability in the intensity in bands at 722 and 1724

$cm^{-1}$, which are due to hypoxanthine, as we can draw by the comparison with hypoxanthine SERS spectrum data (**Figure. 3.2**). Most of the SERS spectra profile can be linked to bilirubin family species, as can be observed by the characteristic bilirubin SERS peak at 785 $cm^{-1}$ [31] [32]. The Principal component analysis (PCA) has been used to get a more complete explanation of SERS dataset variability. The first principal component explains about 55.3% of the spectral variance while the second and third principal components explain respectively only 14.9% and 10.1% of the spectral variance, (Fig. S5 in the Supplementary ref. [1]). As shown with Loadings of the first principal component of the SERS (**Figure. 3.3**), the most part of the variability can be explained with hypoxanthine peaks and xanthine. Bilirubin-like species contribution on spectral variability is marginal and has slight influence on the second principal component (the loadings of the first six principal components are shown in Supplementary material, Figure. S6 ref [1]).

Bilirubin and bilirubin-related species are expected to be present in stools add products of the catabolism of heme group, while xanthine oxidase converts hypoxanthine to xanthine and then to uric acid and can be usually found in urine [34, 35]. Moreover, about 60% of fecal mass is made of bacteria [36] and peaks related to hypoxanthine and xanthine, and other purine metabolites have been observed in SERS dataset of many bacteria [37–40], reinforcing our interpretation of observed SERS spectra profiles.

A recent study by Scott Lee et al. suggested that faecal metabolites could be produced by bacteria, having they observed hypoxanthine and other purines in mice faeces while purines couldn’t be detected in germ-free mice [41]. Therefore, we can suggest hypoxanthine and xanthine peaks present in the SERS spectra of faecal extracts can be related to faecal bacteria instead to host metabolism. Precedent SERS studies [39] highlighted those purines resulting from the metabolic degradation of nucleic acids or nucleotides are secreted by bacteria into extracellular regions, where they enter in contact with plasmonic SERS substrates. As a result, xanthine and hypoxanthine peaks noticed in SERS spectra profiles of faecal extracts are likely related to faecal bacteria secretions containing purine metabolites. This hypothesis is furtherly enforced by the fact that, despite a recent study report that methanol might cause bacterial cell lysis after hours of incubation [42], we can neglect time effect, since sample preparation for

SERS measurements lasts only a few minutes which is not sufficient for bacteria cells lysis.

Mass spectrometry data from previous SERS studies on bacteria also reported the presence in high concentrations of several other kinds of metabolites in the bacteria supernatant [39]. However, only purines related bands are present in SERS profile, as affinity for the metal surface discriminates against which analytes, such as purines which highly interact with Au and Ag surfaces, are observed by SERS spectra and which are not [39]. Purines metal affinity, such as uric acid and hypoxanthine, drives SERS spectra of many biological fluids, such as blood serum, plasma and tears the presence of thousands despite the presence of several other metabolites [43]. We can thus probably suppose a similar effect in case of SERS spectra of faecal extracts, which are rich in hundreds of different metabolites [44, 45]. There seems to be differences in the scores of the first principal component of the SERS dataset of the three different groups which are object to this study (**Figure 3.4**). In fact, gluten-free diet (GFD) might have a considerable effect on spectra, as we can see from GFD group scores differentiation from the other groups. By a direct comparison between the scores of coeliac patients following a gluten-free diet (GFD) or no particular diet (CD), the PC1 scores of the spectra from samples of GFD are significantly higher than CD, meaning that hypoxanthine and xanthine bands shown in **Figure. 3.3** are more intense in the GFD group.

The comparison of the three groups spectra dataset (**Figure. 3.5**) confirms an increased intensity in hypoxanthine band at 722 $cm^{-1}$ in GFD group. The median of the spectral differences between the samples of the GFD and CD groups (**Figure. 3.6**) underlines also a higher relative intensity of a xanthine band, which is supported by the loadings graph in **Figure. 3.3** On the contrary, we can notice the spectral differences between the spectra of the CD and CTR groups are much smaller than those between the spectra of the CD and GFD groups (**Figure. 3.5**).

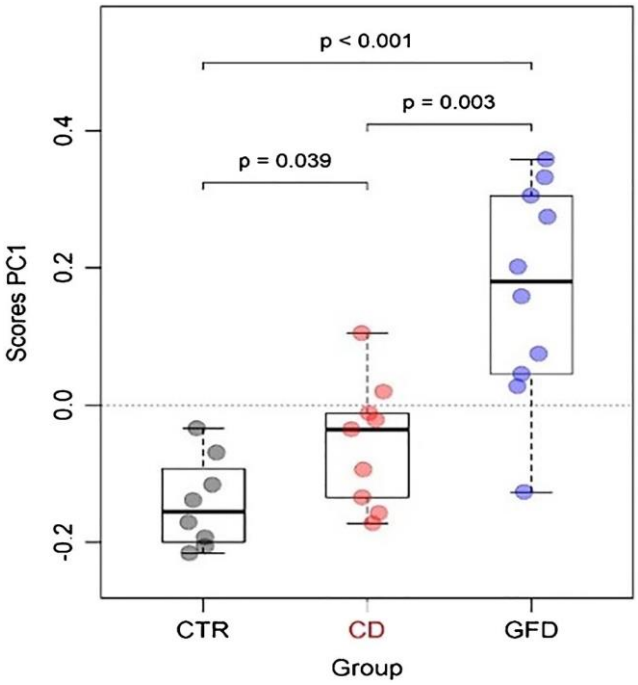


**Figure 3.4** Scores of PC1 of PCA divided by class of patients (controls CTR; coeliac disease CD, gluten-free diet, GFD). The p-value has been obtained with a pairwise t test, without assuming equal variances. Reprinted from [1]

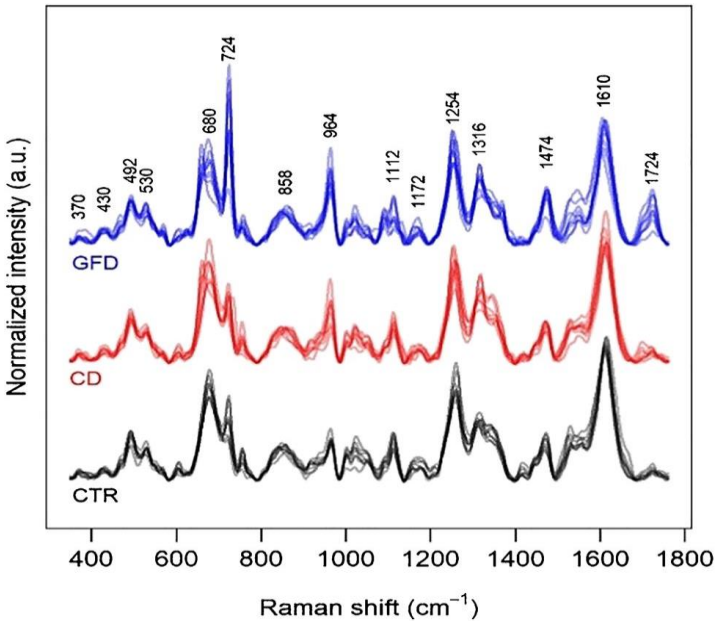


**figure 3.5** Over imposed SERS spectra of focal extract divided by class of patients (controls CTR; coeliac disease CD, gluten-free diet, GFD). AuNP with 785 nm as excitation source. Reprinted form [1].

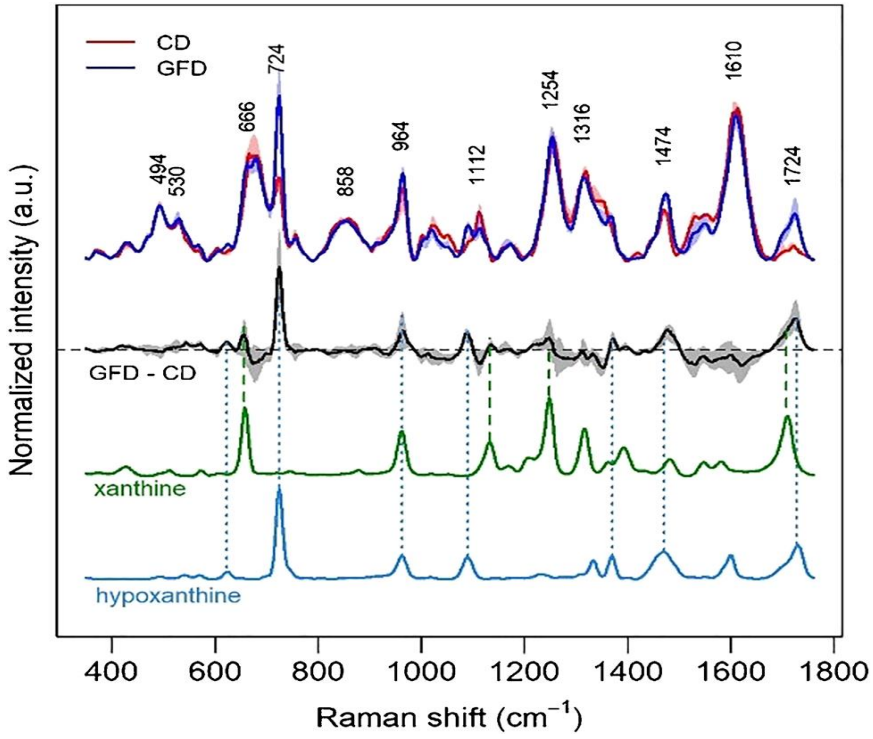


**Figure 3.6** SERS spectra comparison of median and iQR (interquartile range as shaded areas) between the intensity of CD group (red) and GFD group in red (red). Difference spectra GDF -CD black spectra in black (IQR difference is shown as grey shaded area). SERS spectra of Xanthine and Hypoxanthine in the same buffer and experimental condition are reported for comparison in green and light blue respectively. reprinted form [1]

In order to highlight whether these spectral differences are reflecting a different bacterial composition of the faecal samples of the three groups, a microbiota analysis of all samples was conducted by sequencing V4 PCR amplicons from the ribosomal 16S RNA genes. A total of 3,556,159 raw sequences with an average of 107,762 ± 22,119 reads per sample were yield from amplicon sequencing, which were subsequently quality filtered, trimmed from primers and adapters, leaving to 2,377,022 reads. of 250 bp in length. The remaining sequences were reference-based clustered using the SILVA 16S v132 database with a 97% sequence similarity accounting for 2915reference-based OTUs and 1128 de novo OTUs from the 27 tested samples.

The average number of sequences in OTUs was 62,658 ± 7549 for the control, 63,309 ± 11,501 for CD and 72,312 ± 17,413 for GFD samples. Rarefaction curves computed on the total OTU samples reached the plateau indicating that sequencing was representative of the majority of phylotypes in all the samples (Appendix A figure S8 ).

The analysis of the samples at “family” taxonomic level (**Figure 3.7**) showed that in about 75% of the total reads *Lachnospiraceae*, *Ruminococcaceae* (orderClostridiales) and *Bacteroidaceae* (order Bacteroidales) are the most present bacteria families in faecal

samples, which is coherent with the predominance Firmicutes and Bacteroidetes phyla observed in previous studies on gut microbiome composition [46, 47]. On average, a total of 79 genera and 26 prokaryotic families can be recognized in the faecal microbiota, with a variability within each group, being the GFD the most homogeneous.

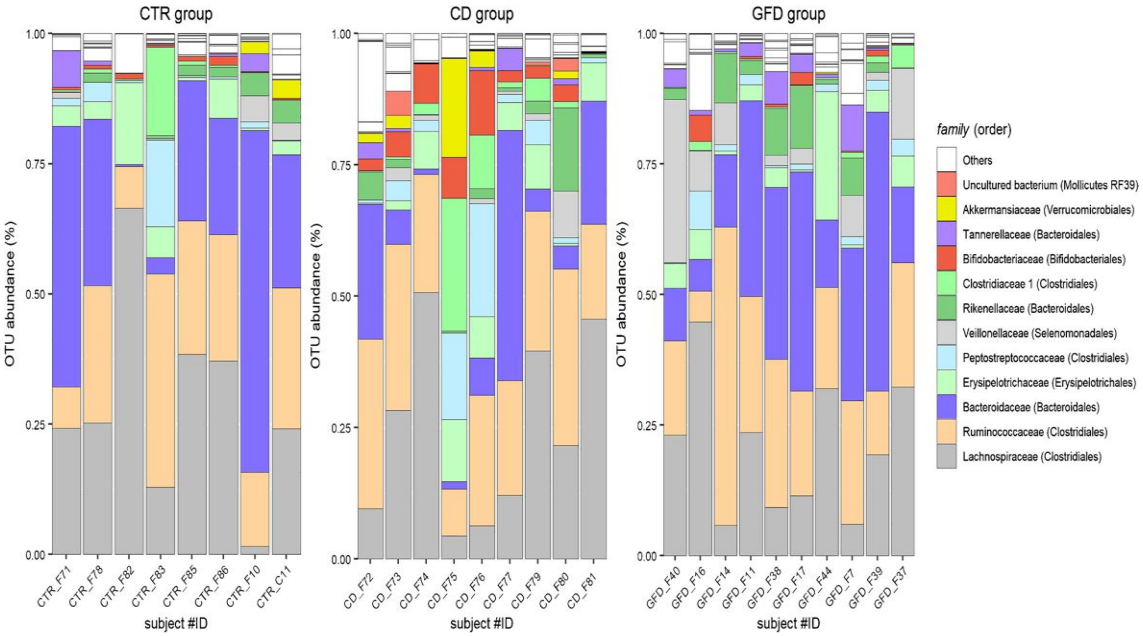


**Figure 3.7** most relative abundant family of bacteria from the OUT's table for the 3 different groups. (Controls CTR group; coeliac disease CD group, gluten-free diet, GFD group). Reprinted from [1]

A PERMANOVA test (**Table 3.2**) shows some significant differences between the three groups. As emerged by SERS Spectra, GFD seems to have a great impact on microbiota, thus we hypnotize that diet may explain spectral and microbiological differences observed between the CD and GFD groups. Nevertheless, we limit our analysis to a descriptive case study conducted on a small number of subjects with ages not perfectly matching in the three groups: we can't thus exclude an effect of age variations between CD and GFD could partly explain these differences as well. Previous literature reported an impact on gut microbiota due to GFD [48, 49], despite there's no clear consensus on the results. In order to better understand which bacteria are responsible for these variations between the groups, a differential abundance analysis has been conducted (Table S9 of the Supplementary Information [1]). It emerged that three families (i.e.an uncultured bacterium from the order of the Mollicutes RF39—phylum Tenericutes, *Akkermansiaceae*—phylum Verrucomicrobia and *Clostridiaceae* 1—phylum Firmicutes) are significantly more present in the CD group than in the GFD group.

**Table 3.2** Permanova test on bryan-curtis distances from OUT's table deriving from 16S rRNA sequencing

| Groups | | Pseudo *f*-statistics | *p* value | |
|---|---|---|---|---|
| CTR, CD, GFD | | 1.367 | 0.040 | |
| Group 1 | Group 2 | Pseudo *f*-statistics | *p* value | *p* value (Bonferroni) |
| CD | CTR | 1.231 | 0.207 | 0.622 |
| CD | GFD | 1.664 | 0.015 | 0.046 |
| CTR | GFD | 1.187 | 0.203 | 0.609 |

**Table 3.3** Spearman's correlation coefficient and FDR values of OUT's relative abundances and PC1 scores of the SERS dataset, for families obtained by the differential abundance analysis

| Name | Correlation coefficient | FDR *p* value |
|---|---|---|
| Uncultured bacterium (Mollicutes) | −0.03 | 0.98 |
| *Akkermansiaceae* | −0.29 | 0.83 |
| *Clostridiaceae 1* | −0.13 | 0.98 |

Genus level comparison showed that *Rikenellaceae* RC9 gut group (order *Bacteroidales*), uncultured bacterium (order Mollicutes RF39) and *Akkermansia* were statistically less represented in GFD subjects than in CD (all with a $p < 0.001$, Bonferroni corrected), while *Escherichia-Shigella* is more represented in the former group, despite the presence of a relevant difference in the GFD-vs-CTRL comparison.

The direct comparison of our results with effects of a GFD on the microbiota of coeliac patients' literature has shown many difficulties, since many studies were performed with several methods, with samples deriving from adults and statistical data analysis approaches [48, 49]. By performing a correlation test between the OTU's relative abundances and the PC1 scores of the SERS dataset for each sample (Table 3) Spearman's clearly evidenced that there is no correlation between SERS spectra and the presence of these nor for other bacterial families. This may suggest that SERS data detect bacterial metabolism rather than bacterial composition of stool samples. Being our study limited to a small group of subjects and going a further study on a wider number of subjects beyond our purpose, we might reasonably hypothesize that the result of the metabolism of the same bacteria may depend on the nutrients present in dietary intake. In this perspective, SERS data of a bacterium doesn't univocally identify the species but it's rather a proof of the bacteria metabolic state. This assumption is in line with Weiss et al. results on SERS spectra of different bacteria while varying metabolic conditions [38], thus also explaining similar number of bacteria species in

stool samples of CD and GFD groups can exhibit different metabolic profiles and really different composition of fecal extracts and ultimately in different SERS spectra. In this frame SERS data can be thought as complementary to that of genomic analysis of 16S rRNA, and has push our hypotheses to be changed, and to consider the SERS data as an indicator of the overall metabolic state of the gut microbiota, rather than the result of a specific bacterial strain responsible for the different metabolic profile of the hypoxanthine among the CD and GFD group. This behavior can be thought because of the biological complexity of the studied system [52-54]. For this reason, why the hypoxanthine level change remains still under debate since no literature studies have never reported the correlation of the hypoxanthine concentration with reduction of gluten intake. At the best of our knowledge, starvation condition in bacteria can increase the production of purine metabolites [38-40][51], but there is no evidence that this metabolic variation occurs in gut microbiota under gluten free diet. However, SERS can show a limited frame of the complexity of the metabolism, even in comparison with standard metabolomic approach. SERS is also highly depending on external variable, like solvent and variation of substrate used for the analysis. Thus, in principle should be possible by varying this factor to expand the available metabolic information. For examples by varying the positively charge SERS surface should be possible increase the affinity for bacterial metabolites. In good agreement with this suggestion Premasiri and colleagues has demonstrated on SERS gold substrate that is possible to bind several bacterial metabolites and to use their spectral differences to create a metabolic signature, showing high sensitivity or the SERS in discriminating this kind of metabolites [40]. This once again, underlines that SERS can be used in a reliable complementary way in tandem with the genomic analysis.

## 3.4 conclusions

Very Consistent SERS spectra form stool samples can be easily obtained by extraction of faecal water in methanol, and by mixing it with gold nanoparticles. We have learned that under this condition that few metabolites are responsible for the SERS spectra in our samples, and main spectral bands are due to bilirubin like species and to purines (like xanthine and hypoxantine), which origin is due to the gut bacteria secretion. But, more interestingly purine bands in SERS spectra have shown a different relative abundance of

these components among the CD and GFD group, suggesting that the gut bacteria metabolism is different in the two group of samples. These differences were not sufficient to explain differences in the composition of bacteria among the two group, as demonstrated by the genomic analysis. But, on the contrary can express a real difference in bacterial metabolism, that can be related to a multifactorial system, due to bacteria interaction, gut physiology, or more simply food ingestion. however, we can consider SERS spectra as informative of the overall metabolic state of gut bacteria, while instead, the genomic analysis can produce punctual information on the diversity of the gut microbiota in different pathological states. Thus, we can conclude that SERS and genomic analysis are two complementary techniques. Finally, this study has shown that SERS spectroscopy can be used to find useful metabolic information form stool samples, with a reliable and simple analytical protocol, but also, if will be confirmed with a larger sample size, that Label-free SERS can be used to assess the compliance of GFD patients.

## Bibliography


1. Fornasaro, Stefano, et al. Spectroscopic investigation of faeces with surface-enhanced Raman scattering: a case study with coeliac patients on gluten-free diet. *Analytical and bioanalytical chemistry*, 2022, 414.11: 3517-3527.
2. Marcobal A, Kashyap PC, Nelson TA, Aronov PA, DoniaMS, Spormann A, Fischbach MA, Sonnenburg JL. A metabolomicview of how the human gut microbiota impacts the host metabolome using humanizedand gnotobiotic mice. ISME J.2013;7:1933–43. https:// doi. org/ 10. 1038/ ismej. 2013. 89.
3. Harmsen HJM, de Goffau Marcus C. The human gut microbiota.In: Schwiertz A, editor. Microbiota of the human body. SpringerInternational Publishing; 2016. p. 95–108.
4. Clarke G, Stilling RM, Kennedy PJ, Stanton C, Cryan JF, Dinan TG. Minireview: gut microbiota: the neglected endocrine organ.Mol Endocrinol. 2014; 28:1221–38. https:// doi. org/ 10. 1210/ me.2014- 1108.
5. Zhu Q, Gao R, Wu W, Qin H. The role of gut microbiota in thepathogenesis of colorectal cancer. Tumor Biol. 2013;34:1285–300. https:// doi. org/ 10. 1007/ s13277- 013- 0684- 4.
6. Silverman GJ, Azzouz DF, Alekseyenko AV. Systemic lupuserythematosus and dysbiosis in the microbiome: cause or effector both? Curr Opin Immunol. 2019;61:80–5. https:// doi. org/ 10. 1016/j. coi. 2019. 08. 007.
7. Wutthi-in M, Cheevadhanarak S, Yasom S, Kerdphoo S,Thiennimitr P, Phrommintikul A, Chattipakorn N, Kittichotirat W, Chattipakorn S. Gut microbiota profiles of treated metabolic syndrome patients and their relationship with metabolichealth. Sci Rep. 2020;10:10085. https:// doi. org/ 10. 1038/s41598- 020- 67078-3.
8. Stokholm J, Blaser MJ, Thorsen J, Rasmussen MA, Waage J, Vinding RK, Schoos A-MM, Kunoe A, Fink NR, Chawes BL, BonnelykkeK, Brejnrod AD, Mortensen MS, Al-Soud WA,

Sorensen SJ,Bisgaard H. Maturation of the gut microbiome and risk of asthmain childhood. Nat Commun. 2018;9:141. https:// doi. org/ 10. 1038/s41467- 017- 02573-2.
9. Sharon G, Sampson TR, Geschwind DH, Mazmanian SK.The central nervous system and the gut microbiome. Cell.2016;167:915–32. https:// doi. org/ 10. 1016/j. cell. 2016. 10. 027.
10. Poretsky R, Rodriguez-R LM, Luo C, Tsementzi D, KonstantinidisKT. Strengths and limitations of 16S rRNA gene ampliconsequencing in revealing temporal microbial community dynamics.PLoS One. 2014;9:e93827. https:// doi. org/ 10. 1371/ journ al. pone.00938 27.
11. Cialla-May D, Zheng X-S, Weber K, Popp J. Recent progressin surface-enhanced Raman spectroscopy for biological andbiomedical applications: from cells to clinics. Chem Soc Rev.2017;46:3945–61. https:// doi. org/ 10. 1039/ C7CS0 0172J.
12. Premasiri WR, Chen Y, Fore J, Brodeur A, Ziegler LD. SERS biomedicalapplications: diagnostics, forensics, and metabolomics.In: Laane J, editor. Frontiers and advances in molecular spectroscopy.Elsevier; 2018, pp 327–367.
13. Comino I, Real A, Vivas S, Siglez MA, Caminero A, Nistal E,Casqueiro J, Rodriguez-Herrera A, Cebolla A, Sousa C. Monitoringof gluten-free diet compliance in celiac patients by assessmentof gliadin 33-mer equivalent epitopes in feces. Am J Clin Nutr.2012;95:670–7. https:// doi. org/ 10. 3945/ ajcn. 111. 026708.
14. Sellitto M, Bai G, Serena G, Fricke WF, Sturgeon C, Gajer P,White JR, Koenig SSK, Sakamoto J, Boothe D, Gicquelais R, Kryszak D, Puppa E, Catassi C, Ravel J, Fasano A. Proof ofconcept of microbiome-metabolome analysis and delayed glutenexposure on celiac disease autoimmunity in genetically at-riskinfants. PLoS One. 2012;7:e33387. https://d oi. org/ 10. 1371/ journal. pone. 00333 87.
15. Verdu EF, Galipeau HJ, Jabri B. Novel players in coeliac diseasepathogenesis: role of the gut microbiota. Nat Rev GastroenterolHepatol. 2015;12:497–506. https:// doi. org/ 10. 1038/ nrgas tro. 2015.90.
16. Leonard MM, Karathia H, Pujolassos M, Troisi J, Valitutti F, SubramanianP, Camhi S, Kenyon V, Colucci A, Serena G, CucchiaraS, Montuori M, Malamisura B, Francavilla R, Elli L, Fanelli B,Colwell R, Hasan N, Zomorrodi AR, Fasano A, the CD-GEMM Team, Piemontese P, Calvi A, Baldassarre M, Norsa L, TrovatoCM, Raguseo CL, Passaro T, Roggero P, Crocco M, Morelli A,Perrone M, Chieppa M, Scala G, Lionetti ME, Catassi C, Serretiello A, Vecchi C, de Villsante GC. Multi-omics analysis revealsthe influence of genetic and environmental risk factors on developinggut microbiota in infants at risk of celiac disease. Microbiome.2020;8:130. https:// doi. org/ 10. 1186/ s40168- 020- 00906- w.
17. Turkevich J, Stevenson PC, Hillier J. A study of the nucleation and growth processes in the synthesis of colloidal gold. DiscussFaraday Soc. 1951;11:55. https:// doi. org/ 10. 1039/ df951 11000 55.
18. R Core Team (2021). R: a language and environment for statistical computing. R Foundation for Statistical Computing, Vienna, Austria. https:// www.R- proje ct. org/.
19. Beleites C, Sergo V. HyperSpec: a package to handle hyperspectral data sets in R. R Package Version 099–20200527. 2020.https:// github. com/ cbele ites/ hyper Spec.
20. Liland KH, Almoy T, Mevik B-H. Optimal choice of baseline correction for multivariate calibration of spectra. ApplSpectrosc. 2010;64:1007–16. https:// doi. org/ 10. 1366/ 0003702107 92434 350.

21. Asuero AG, Sayago A, Gonzalez AG. The correlation coefficient: an overview. Crit Rev Anal Chem. 2006;36:41–59. https:// doi. org/10. 1080/ 10408 34050 05267 66.
22. Benjamini Y, Hochberg Y. Controlling the false discovery rate: a practical and powerful approach to multiple testing. J R StatSoc Ser B Methodol. 1995;57:289–300. https:// doi. org/ 10. 1111/j.2517- 6161. 1995. tb020 31.x.
23. Giglio A, Vommaro ML, Gionechetti F, Pallavicini A. Gut microbial community response to herbicide exposure in a ground beetle. J ApplEntomol. 2021;145:986–1000. https:// doi. org/ 10. 1111/ jen. 12919.
24. Caporaso JG, Lauber CL, Walters WA, Berg-Lyons D, LozuponeCA, Turnbaugh PJ, Fierer N, Knight R. Global patterns of 16SrRNA diversity at a depth of millions of sequences per sample.Proc Natl Acad Sci. 2011;108:4516–22. https:// doi. org/ 10. 1073/pnas. 10000 80107.
25. Quast C, Pruesse E, Yilmaz P, Gerken J, Schweer T, Yarza P, PepliesJ, Glockner FO. The SILVA ribosomal RNA gene databaseproject: improved data processing and web-based tools. NucleicAcids Res. 2012;41:D590–6. https:// doi. org/ 10. 1093/ nar/ gks12 19.
26. Anderson MJ. A new method for non-parametric multivariateanalysis of variance: non-parametric MANOVA for ecology. Austral Ecol. 2001;26:32–46. https:// doi. org/ 10. 1111/j. 1442- 9993.2001. 01070. pp.x.
27. Jafari M, Ansari-Pour N. Why, when and how to adjust your pvalues? Cell J. 2019;20(4):604–7. https:// doi. org/ 10. 22074/ cellj.2019. 5992.
28. Noble WS. How does multiple testing correction work? Nat Biotechnol.2009;27:1135–7. https:// doi. org/ 10. 1038/ nbt12 09- 1135.28. Lin H, Peddada SD. Analysis of microbial compositions: a review of normalization and differential abundance analysis.NPJ Biofilms Microbiomes. 2020;6:60. https:// doi. org/ 10. 1038/s41522- 020-00160-w.
29. Cui M, Trimigno A, Aru V, Khakimov B, Engelsen SB. Human faecal 1 H NMR metabolomics: evaluation of solvent and sampleprocessing on coverage and reproducibility of signature metabolites.Anal Chem. 2020;92:9546–55. https:// doi. org/ 10. 1021/ acs.
30. Lin H, Peddada SD. Analysis of microbial compositions: areview of normalization and differential abundance analysis.NPJ Biofilms Microbiomes. 2020;6:60. https:// doi. org/ 10. 1038/s41522- 020- 00160-w.
31. Cui M, Trimigno A, Aru V, Khakimov B, Engelsen SB. Humanfaecal 1 H NMR metabolomics: evaluation of solvent and sampleprocessing on coverage and reproducibility of signature metabolites.Anal Chem. 2020;92:9546–55. https:// doi. org/ 10. 1021/ acs.analc hem. 0c006 06.
32. Koya SK, Yurgelevic S, Brusatori M, Huang C, Diebel LN, Auner GW. Rapid detection of Clostridium difficile toxins in stool byRaman spectroscopy. J Surg Res. 2019;244:111–6. https:// doi. org/10. 1016/j. jss. 2019. 06. 039.
33. Ouyang L, Yao L, Tang R, Yang X, Zhu L. Biomimetic point-ofcare testing of trace free bilirubin in serum by using glucose selectivecapture and surface-enhanced Raman spectroscopy. SensorsActuators B Chem. 2021;340:129941. https:// doi. org/ 10. 1016/j.snb. 2021. 129941.
34. Vu TD, Jang E, Lee J, Choi D, Chang J, Chung H. Feasibility ofvoltage-applied SERS measurement of bile juice as an effectiveanalytical scheme to enhance discrimination between gall bladder (GB) polyp and GB cancer. Anal Chem. 2020;92:8159–69. https://doi. org/ 10. 1021/ acs. analc hem. 0c002 75.

35. Hamoud A-R, Weaver L, Stec DE, Hinds TD. Bilirubin in theliver–gut signaling axis. Trends Endocrinol Metab. 2018;29:140–50. https:// doi. org/ 10. 1016/j. tem. 2018. 01. 002.
36. Sorensen LB. Role of the intestinal tract in the elimination of uricacid. Arthritis Rheum. 1965;8:694–706. https:// doi. org/ 10. 1002/art. 17800 80429.
37. Hosomi A, Nakanishi T, Fujita T, Tamai I. Extra-renal eliminationof uric acid via intestinal efflux transporter BCRP/ABCG2. PLoSOne. 2012;7:e30456. https:// doi. org/ 10. 1371/ journ al. pone. 00304 56.
38. Stephen AM, Cummings JH. The microbial contribution to humanfaecal mass. J Med Microbiol. 1980;13:45–56. https:// doi. org/ 10.1099/ 00222 615- 13-1- 45.
39. Chiu SW-Y, Cheng H-W, Chen Z-X, Wang H-H, Lai M-Y, Wang J-K, Wang Y-L. Quantification of biomolecules responsible for biomarkersin the surface-enhanced Raman spectra of bacteria usingliquid chromatography-mass spectrometry. Phys Chem Chem Phys.2018;20:8032–41. https:// doi. org/ 10. 1039/ C7CP0 7103E.
40. Weiss R, Palatinszky M, Wagner M, Niessner R, Elsner M, SeidelM, Ivleva NP. Surface-enhanced Raman spectroscopy of microorganisms:limitations and applicability on the single-cell level.Analyst. 2019;144:943–53. https:// doi. org/ 10. 1039/ C8AN0 2177E.
41. Premasiri WR, Lee JC, Sauer-Budge A, Theberge R, CostelloCE, Ziegler LD. The biochemical origins of the surface-enhanced Raman spectra of bacteria: a metabolomics profiling by SERS.Anal Bioanal Chem. 2016;408:4631–47. https:// doi. org/ 10. 1007/s00216- 016- 9540-x.
42. Kubryk P, Niessner R, Ivleva NP. The origin of the band at around 730 cm −1 in the SERS spectra of bacteria: a stable isotopeapproach. Analyst. 2016;141:2874–8. https:// doi. org/ 10.1039/ C6AN0 0306K.
43. Lee JS, Wang RX, Goldberg MS, Clifford GP, Kao DJ, Colgan SP. Microbiota-sourced purines support wound healing and mucous barrier function. iScience. 2020;23:101226. https:// doi. org/ 10.1016/j. isci. 2020. 101226.

42 Zhu L, Rajendram M, Huang KC. Effects of fixation on bacterial cellular dimensions and integrity. iScience. 2021;24:102348.https:// doi. org/ 10. 1016/j. isci. 2021. 102348.

44. Bonifacio A, Cervo S, Sergo V. Label-free surface-enhanced Raman spectroscopy of biofluids: fundamental aspects and diagnosticapplications. Anal Bioanal Chem. 2015;407:8265–77.https:// doi. org/ 10. 1007/ s00216- 015- 8697-z.
45. Karu N, Deng L, Slae M, Guo AC, Sajed T, Huynh H, Wine E,Wishart DS. A review on human fecal metabolomics: methods,applications and the human fecal metabolome database. AnalChim Acta. 2018;1030:1–24. https:// doi. org/ 10. 1016/j. aca. 2018.05. 031.
46. Zierer J, Jackson MA, Kastenmuller G, Mangino M, Long T, TelentiA, Mohney RP, Small KS, Bell JT, Steves CJ, Valdes AM,Spector TD, Menni C. The fecal metabolome as a functional readoutof the gut microbiome. Nat Genet. 2018;50:790–5. https:// doi.org/ 10. 1038/ s41588- 018- 0135-7.
47. MetaHIT Consortium (additional members), Arumugam M, RaesJ, Pelletier E, Le Paslier D, Yamada T, Mende DR, Fernandes GR,Tap J, Bruls T, Batto J-M, Bertalan M, Borruel N, Casellas F,Fernandez L, Gautier L, Hansen T, Hattori M, Hayashi T, KleerebezemM, Kurokawa K, Leclerc M, Levenez F, Manichanh C,Nielsen HB, Nielsen T, Pons N, Poulain J, Qin J, Sicheritz-Ponten T, Tims S, Torrents D, Ugarte E, Zoetendal EG, Wang J, GuarnerF, Pedersen O, de Vos WM, Brunak S, Dore J, Weissenbach J,Ehrlich SD, Bork P.

Enterotypes of the human gut microbiome.Nature. 2011;473:174–80. https:// doi. org/ 10. 1038/ natur e09944.

48. Lozupone CA, Stombaugh JI, Gordon JI, Jansson JK, Knight R.Diversity, stability and resilience of the human gut microbiota.Nature. 2012;489:220–30. https:// doi. org/ 10. 1038/ natur e11550.48. Caio G, Lungaro L, Segata N, Guarino M, Zoli G, Volta U, DeGiorgio R. Effect of gluten-free diet on gut microbiota composition in patients with celiac disease and non-celiac gluten/wheatsensitivity. Nutrients. 2020;12:1832. https:// doi. org/ 10. 3390/nu120 61832.
49. Polo A, Arora K, Ameur H, Di Cagno R, De Angelis M, GobbettiM. Gluten-free diet and gut microbiome. J Cereal Sci.2020;95:103058. https:// doi. org/ 10. 1016/j. jcs. 2020. 103058.
50. Link H, Fuhrer T, Gerosa L, Zamboni N, Sauer U. Real-timemetabolome profiling of the metabolic switch between starvationand growth. Nat Methods. 2015;12:1091–7. https:// doi. org/ 10.1038/ nmeth. 3584.
51. Ponomarova O, Patil KR. Metabolic interactions in microbialcommunities: untangling the Gordian knot. Curr Opin Microbiol.2015;27:37–44. https:// doi. org/ 10. 1016/j. mib. 2015. 06. 014.
52. Cavaliere M, Feng S, Soyer OS, Jimenez JI. Cooperation in microbialcommunities and their biotechnological applications. EnvironMicrobiol. 2017;19:2949–63. https:// doi. org/ 10. 1111/ 1462- 2920.13767.
53. Ang KS, Lakshmanan M, Lee N-R, Lee D-Y. Metabolic modelingof microbial community interactions for health, environmental andbiotechnological applications. Curr Genomics. 2018;19:712–22.https:// doi. org/ 10. 2174/ 13892 02919 66618 09111 44055.
54. Erben V, Poschet G, Schrotz-King P, Brenner H. Evaluationof different stool extraction methods for metabolomicsmeasurements in human faecal samples. BMJ Nutr PrevHealth. 2021:bmjnph-2020–000202. https:// doi. org/ 10. 1136/bmjnph- 2020-000202.
55. Freeman HJ. Dietary compliance in celiac disease. World J Gastroenterol. 2017;23:2635. https:// doi. org/ 10. 3748/ wjg. v23. i15.2635.
56. Moreno M, Rodriguez-Herrera A, Sousa C, Comino I. Biomarkers to monitor gluten-free diet compliance in celiac patients. Nutrients. 2017;9:46. https:// doi. org/ 10. 3390/ nu901 0046.

# 4. A protocol study on human serum for Label free SERS biosensing: the centrifugal silver plasmonic paper (CSPP) sampling methodology

## 4.1Introduction:

SERS (Surface Enhanced Raman scattering) spectroscopy is a powerful analytical technique that combines easy and rapid data acquisition with high sensitivity and specificity in chemical species recognition. The capability, in Raman spectroscopy of identifying molecular species is usually referred as *vibrational fingerprinting* and is obtained by recording specific vibrational modes of sampled molecules. Specifically, in SERS, metal nanostructured surfaces with proper plasmonic features can enhance of several orders of magnitude the Raman signal intensity of adsorbing molecules, by hot-spots formation in which LSPRs (localized surface plasmon resonance) are generated as previously reported in the chapter 2.

These plasmonic surfaces (SERS substrates) are often thought to be ad-hoc devices developed for specific analytical issues or, in other words, readily recognize a unique molecule of interest. Such specificity might be reached by tuning plasmonic structures and through their chemical functionalization [1]. Specifically, adding ligands or reporter molecules is possible also a femtomolar level quantitation [2]. However, to fit the analytical needs, especially in term of specificity is required a remarkable effort to study and optimize the superficial chemistry. We can refer to these SERS applications as labelled or targeted.

Differently, even very promising SERS label-free applications are emerging to analyse probing molecules directly. In the label-free Approach particularly, molecules that freely absorb on metal surfaces can generate an intense SERS signal. Thus, in principle, might be possible to identify several putative biomarkers, exploiting an uncommon multiplexing ability [3], just accounting on the affinity between the molecules and metal surface. But this can be an arduous task, above all in complex

samples in which hundreds of molecules can generate the same or overlapping spectral bands, making bands attribution almost impossible.

On the contrary, especially for biomedical or bioanalytical applications in biofluid, that are the topic of this section, the plasmonic metal surface act as strong and effective filter reducing the number of molecules responsible in the SERS signal generation. Interestingly, these molecules seem to be less to what expected, allowing to reproduce the spectra using very few pure components [4]. Thus, label-free SERS can be considered a valuable approach to investigate a set of metabolites in several biofluids, with each spectrum representing a sort of “metabolic fingerprint” [5].

In addition, this metabolomic approach in precision medicine has received a recent boost, thanks to the identification of several biological targets, ranging from cells receptor to non-coding RNA, that have shown to be a good predictor of different pathological states for several pathologies in biofluid [6]. Thus, on this base several studies have been started to develop “liquid biopsy” approaches, as alternative to surgery diagnostic and prognostic tools [7]. Specifically, serum and plasma are largely used in liquid biopsy to detect the presence or quantify metabolites and small molecules as diagnostic or prognostic biomarkers.

For this analytical purpose, several label-free SERS pre-clinical studies on serum and plasma have been performed, suggesting the possibility of SERS spectroscopy to monitor and diagnose liver and breast cancer [8] [9], and to monitor the blood concentration of antitumoral drugs [10]. Thus, it is possible to exploit the SERS unique analytical features, among them we have the fast and user-friendly data acquisition can make the difference on the other analytical techniques in use as clinical standards [11].

In this context, different SERS substates have been developed for these label-free applications. The most common production methods reside in the chemical synthesis of colloidal suspension of gold and silver nanoparticles in aqueous media [12][13]. In these colloidal substrates a strong LSPs interaction is obtained by NPs aggregation in presence of analytes. Alternatively, depositing pre-aggregated or aggregating nanoparticles on different types of supports, commonly porous silicon or paper [14] [15], is a common approach to produce solid and flexible substrates, respectively. These systems allow a more stable and controlled distribution of metal nanoparticles that passively interact with adsorbing molecules. While, on the contrary,

in colloidal system it is arduous to control adequately the NPs aggregation of the colloids-sample mixture, providing high level of SERS signal variability, due to the presence of a different hot-spots concentration and large aggregate precipitation.

Particularly, SERS paper-based substrates, or more commonly plasmonic papers has gained importance in both number of applications and production techniques, thanks to their general inexpensive and easy production procedures. These aspects well meet the SERS label-free analytical “vocation” that aims to produce a point-of-care technique, with compact and portable instrumentation, allowing fast, user friendly and cheap campaign of measure.

Thus, paper offers the opportunity to produce flexible, disposable, and inexpensive SERS substrates, but with two main limitations: high variability and a relatively low throughput of fabrication. These factors have limited a real commercial application of plasmonic papers in the SERS analytical field, although they remain a viable tool at the laboratory scale. In this context, nanoparticles in situ growth and post-immobilization are the two more common methods to produce plasmonic papers. In the latter method, nanoparticles are produced using the cellulose matrix as a 3D scaffold, and its lateral chains as reducing agents for silver and gold salts [16]. The Post immobilization process can be achieved by different methods: dip-coating [17][18], filtration [19], printing, and vapor deposition [20]. Thus, it is possible to adapt the fabrication process for specific analytical needs [21]. Among the proposed post-immobilization process, printing and vapor deposition allow the fabrication of very uniform substrates, but with a rise in costs of fabrication and in the complexity of equipment required [22]. Interesting results have been obtained by writing plasmonic ink on paper [23] [24], with a fountain pen, granting a high deposition uniformity and high production throughput [25]. For a schematic evaluation of plasmonic paper, and for a general overview, in Table 4.1 and Table 4.2 are reported a comparison between conventional substrates and paper-based, of the main features to consider in selecting a proper SERS substrate, and the pros and cons of different available SERS paper substrates, respectively.

**Table 4.1** Comparison of selective criteria for Plasmonic paper and conventional SERS substrates, reprinted from [14].

| Criteria | Plasmonic paper | Conventional rigid substrate |
|---|---|---|
| Flexibility | Yes | No |
| Onsite sampling | Yes | Not suitable |
| Additional functionalities | Yes | Not suitable |
| Cost | Lower | Higher |
| Manufacturing throughput | Depends on the fabrication method | Higher |
| Reproducibility | Lower-Medium | Medium- Higher |
| transfer of liquid/ solvent | Wicking of paper allows passive transport of solvent which avoids the use of pipette | Not suitable for passive transfer of liquids |
| Sampling | Very convenient to take sample through swabbing or as a dipstck | not suitable for point-of-sample applications |
| Average EF | $10^6$–$10^8$ | $10^6$–$10^8$ |

**Table 4.2** Plasmonic paper fabrication methods evaluation, reprinted from [14]

| Synthetic Method | Pros | Cons |
|---|---|---|
| In-situ | • the cellulose surface could be used as a self-sacrificing reducing agent (avoids the use of reducing agents)<br>• simple and direct<br>• lower energy and material requirement | • do not allow size and shape tunablity of NPs<br>• difficult to control hotspot density<br>• non reproducible substrates<br>• low manufacturing throughput<br>• requires optimization of multiple solution parameters |
| Dip-coating | • simple, rapid<br>• allows size and shape tunablity of NPs<br>• can be useful for simple qualitative experiments<br>• lower energy and material requirement | • low degree of reproducibly of substrates<br>• low manufacturing throughput<br>• difficult to control hotspot density |
| Printing | • high manufacturing throughput<br>• uniform (reproducible) substrates<br>• allows substrate patterning to incorporate additional analytical functionalities on the same substrate<br>• allows size and shape tunablity of NPs | • requires modification / concentration of nanoparticles ink |
| Physical vapor deposition | • uniform substrates | • high-power and expensive equipment requirement<br>• don't allow size and shape tunablity of NPs |

But none or few of these methods have been applied in label-free SERS biofluid analysis, in which the complexity of the biological samples can be a non-trivial aspect to be tackled, in term of chemical-physical environment and presence of possible disturbing factors at nano-bio interface [26]. As a proof of that, protein-rich biofluids, like serum needs to be filtered to remove the protein content, in SERS label-free

applications. This phenomenon is known as protein corona effect, in which hot-spot formation is hindered by a protein layer [27].

Hence, we have developed a novel protocol for label-free SERS serum sampling, based on a plasmonic paper approach, and able with a single step to produce intense and reliable SERS serum spectra. Precisely, in our method the post-immobilization process of silver colloidal NPs is achieved by centrifugation on a biofluid pre-rinsed paper strip.

## 4.2 Experimental section

### Materials and regents

Sulphuric and nitric acid for glassware cleaning was purchased by VWR (Avantor, USA). All reagents for nanoparticles synthesis were purchased by Sigma-Aldrich (Merk, Germany). Synthesis of silver nanoparticles and water solution were made in ultrapure Water, MilliQ (Millipore, USA). Ergothioneine and hypoxanthine for SERS analysis were purchased by Apollo Scientific (Cheshire, UK) and Sigma-Aldrich (Merck, Germany), respectively.

### Silver nanoparticle Synthesis and characterization

Prior the synthesis all the glassware was cleaned with a sulphuric acid Nochromix® (Godax Laboratories, Inc.) solution, and nitric acid to remove organic and silver metal residues, respectively, and finally thoroughly rinsed with MilliQ water. The silver nanoparticles were synthesized following the Lee-Meisel protocol [8] of chemical reduction of a silver nitrate in water. Briefly, 45mg of $AgNO_3$ were added to 250 ml of water in a flask and heated until boiling. The chemical reduction was achieved adding dropwise 5 ml of sodium citrate tribasic dihydrate solution (1%, g/ml) in water while keeping boiling for 1 hour under vigorous stirring and water condenser reflux. Ultimately, the silver colloidal dispersion was left to cool down at room temperature and conserved in the dark until use. Nanoparticles have been characterized by UV-visible spectroscopy (Cary100, Agilent, Santa Clara, USA).

### Serum filtration protocol

An aliquot 1 ml of serum was thawed and split in two centrifugal ultrafiltration tubes (Amicon, USA, 3 kDa cut off), previously rinsed with 1ml of MilliQ water, and then

centrifuged for 30 minutes. The filtered serum was added to a paper strip following the CSPP protocol presented in the next method section.

Protocol for CSPP sampling methodology

High quality filter paper (Whatman, 2 µm averaged porosity) was used, and cut to strips (0.2x2cm), as in **figure 4.5**. Human serum (from human male AB plasma, USA origin, sterile-filtered) was purchased from sigma-Aldrich (Merk, Germany), divided into aliquots and stored at -20°C. Serum aliquots were thawed at RT and kept in ice, and 2 µl were added to the lid of an Eppendorf tube and absorbed by capillarity through the paper short edge for 30 second. The paper strips with the serum were left to dry for 20 minutes and were put into Eppendorf centrifugal tubes containing 150 µl of silver colloid, with the serum-dipped part pointing toward the bottom of the Eppendorf, and then centrifuged at 4300 x g for 20 minutes in a bench centrifuge (MiniSpin, Eppendorf, USA) to obtain a CSPP. After the centrifugation the CSPP was left to dry for 20 minutes prior to SERS analysis.

SERS spectral acquisition and data processing.

SERS spectra were collected with a portable I-Raman plus spectrometer (B&W Tek, USA) equipped with a 785 nm Laser (output 400 mW) and connected with a compact microscope mounting an Olympus optics 20x (N.A. 0.25, working distance 8.8 mm) with a spot of 108µm. For data collection, the laser power was reduced to 5% (18mW) and an exposure time of 10 s was used to avoid sample photodegradation. Spectra from 10 different spots were randomly collected for each CSPP (from the grey region, indicating the presence of c-AgNP aggregates as shown in **Figure 4.5**), and averaged to accommodate intra-substrate variability. Spectra were imported and processed using R studio software, and the hyperSpec package [28]. Briefly, spectra were cropped, smoothed and interpolated using the spc.loess function (n=2.5, spectral range=400-1800 $cm^{-1}$) of the hyperSpec package, and a polynomial baseline was subtracted using *spc.fit.poly.below* function (poly.order=5). Subsequently the rubber-band hyperSpec function (noise=100, df=10) was applied to reduce distortion of the spectra at the edge. As a secondary pre-processing approach, parallelly used, was applied to test the introduction of spectral artifacts. Thus, the Als function (lambda=4, p=0.001) from the Baseline R package [29] for spectral smoothing and baseline

correction was applied. The two processing procedures yielded a very similar outcome, so they have been used indifferently. The spectral intensity was normalized with a vector normalization when expressed.

Serum collecting system shelf-life

To evaluate the collecting system shelf-life in term of SERS signal durability, 1 ml of serum was thawed, kept on ice, and used to spot different strips as reported in the CSSP protocol section. Thus, the serum strips were left to dry 20 minutes and then stored in parafilm sealed Eppendorf tubes at 4°C. Prior to the SERS analysis the serum strips were centrifuged with the silver colloids and prepared following the CSSP protocol presented above. The shelf-life was assessed up to 2 months. Measurements were performed at 4, 16, 24, 216, 384, 720, 1000 hours with three strips for each time tested and 3 replicate for each strip.

Linear regression model and method optimization

The CSPP sampling protocol presents several parameters to be considered, which can change SERS spectra features, particularly spectra have shown a low intensity and high level of background due to cellulose Raman bands. To understand which parameters were mostly impacting spectra, we have performed a linear regression model whit 6 different procedural parameter as a factor with 2 or 3 level each, that are shown in **Table 4.1**. Hence, we have chosen two different response variables: uric acid band integrated area (620-660$cm^{-1}$) and the cellulose band (1020-1100$cm^{-1}$) to study lack of intensity and level of background, respectively. Prior to perform the linear model, we have applied a D-optimal design algorithm [30], using DoE tool in CAT's routine for R [31] to reduce the numbers of experiment. The matrix with the candidate point is not shown, on the contrary the matrix with optimal point is reported in Appendix A, Table S11. Linear model equation is reported in Eq. 4.1. linear model results are presented in Appendix A, figure S12. Model validation dataset (run 8,19) for each response variable was selected by the dominating point of pareto front, that maximise SERS spectral goodness (low paper cellulose Raman band and high metabolites signal). Model validation results are reported in Figure S13 Appendix A. Pareto front and validation data set spectra are reported in **figure 4.3.**

Pure metabolites serum spiking protocol

2 ml of serum were thawed and kept on ice to prepare the appropriate dilutions with ergothioneine and hypoxanthine. i) A 5 mM ergothioneine stock solution was prepared in water. 4 µl of the stock solution were added to 396 µl of serum to obtain a 50 µM serum Erg-spiked stock solution. Diluted spiked solutions at 25 µM,10 µM, and 5 µM were obtained by 2-fold,5-fold,10-fold diluting in serum the 50 µM stock, respectively. ii) 10mM hypoxanthine solution was prepared in $H_2O$ from 50 mM stock solution in 0.25 mM NaOH, by a 5-fold dilution. An initial 100 µM Hypoxanthine solution was prepared adding 4 µl of 10 mM solution to 396 µl of serum. 50 µM, 25 µM and 10 µM dilutions was obtained by diluting the initial solution in serum 2-fold,4-fold, and 10-fold respectively. Not-spiked serum was used as blank.

## 4.3 Result and Discussion

The present study was inspired by a recent one on periodontal disease [32], performed with a similar methodology, using a very specific commercial paper (Periopaper®) on gingival crevicular fluid (GCF). This biofluid has yielded intense SERS spectra after centrifuging the spotted paper with silver colloids. GCF has a composition close to that of serum, but with a lower concentration of proteins [30]. Surprisingly, the same approach on serum has yielded very similar SERS spectra, with just few differences in the spectrum intensity between filtered and unfiltered samples, as shown in **figure 4.2**. These spectra closely resemble those previously reported on filtered serum [26].

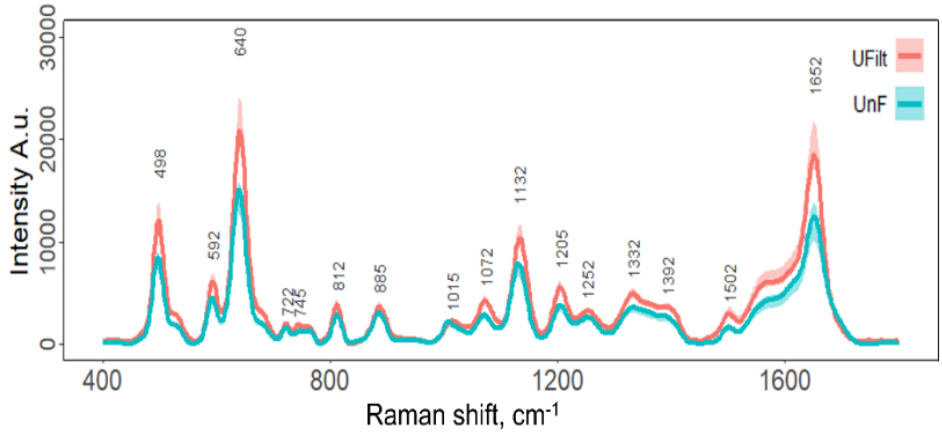


***Figure 4.2*** CSPP with filtered and unfiltered serum: SERS spectra: median and IQR range, of filtered and unfiltered serum on CSPP substrate in red and cyan, respectively.

The spectral similarity permits to describe the metabolic composition of CSPP serum SERS spectra also: an intense band of uric acid at 640cm-1 and a minor band of hypoxanthine at 724 $cm^{-1}$ are clearly visible [17], as reported in **figure 4.2**. The variation in relative intensity in these bands has been reported as a key spectral feature to interpretate the spectral variability between pathological states of patients in several SERS Label-free bioanalytical studies on serum.

A higher relative intensity of the hypoxanthine band, however, is often present in the SERS spectra previously reported in literature. A possible explanation can reside in the origin of serum used in our study. It is a commercial standard pooled SERUM and was collected from American male donors. Thus, it possible to have a different composition to what observed in serum from patients in literature, since no metabolite standardization or quantification is available for commercial serum [24]. However, as shown by Premasiri and colleagues [5], differences in the storage of blood samples can alter the final concentration of hypoxanthine, clearly impacting SERS spectra. As proof of that, fresh whole blood SERS spectra yielded a similar relative intensity of 724$cm^{-1}$ band to the CSSP spectra, using solid gold substrates.

These results show that our method works for protein-rich biofluids as well, overcoming the problem presented by the protein corona hindering the formation of functional aggregates [40] in the case of colloidal substrates. On the contrary, this aspect does not seem to be an important issue for plasmonic paper. In fact, as reported in Gurion et al. [26] in a recent work by our group, the high protein concentration does not affect the intensity of reported SERS serum spectra. Even if, to produce very similar spectra to those obtained with CSPP methodology has been apply a more complex and time-consuming approach, for serum reference SERS spectra obtained with different methods see Appendix A, Figure S15. Thus, the proposed dip-coating plasmonic paper production protocol needs of 10-fold concentrated silver nanoparticles to be added to the paper together with sodium citrate salt to be less sensible to the protein content. Eventually, other procedural issues can be also found, like the inter-substrates reproducibility, since to improve the coating efficiency only small paper substrates can be treated on the same spot. Additionally, colloidal systems are prone to exhibit a low batch-to-batch reproducibility by themself. But more specifically, dip-coated plasmonic

paper production throughput is the main disadvantage of the method proposed in [10], considering the several days of paper soaking into the colloidal solution.

Thus, once achieved the possibility to obtain SERS spectra from unfiltered serum with this easy-to-use sampling protocol, a method evaluation and optimization has been performed. Specifically, we have carefully studied: i) the procedural variables impact on serum metabolites SERS signal, with a multivariate linear regression model (parameters and method optimization). ii) the system reproducibility (as RSD of SERS serum signal inter-CSPP); iii) the spectral analytical reliability (in term of sensitivity to the addition of SERS serum known pure components); iv) the durability of the collecting system (shelf-life of the serum spotted strip evaluated as serum metabolites SERS signal).

Table *4.1* procedural variables and level selected for protocol optimization

| Factor | Symbol | Levels | | |
|---|---|---|---|---|
| Analyte drying time (min) | A | 0 | - | 20 |
| Ag-NPs volume (µL) | B | 75 | 100 | 150 |
| Incubation time (min) | C | 0 | - | 20 |
| Centrifugation time (min) | D | 2 | 10 | 20 |
| Centrifugation speed (rpm) | E | 4000 | 8000 | 13,000 |
| Drying time after centrifugation (min) | F | 0 | - | 20 |

$$Y = 4.97 - 0.61\mathrm{A} - 0.37\mathrm{B} + 0.80\mathrm{C} + 1.82\mathrm{D}^{(**)} - 0.54\mathrm{E} + 2.01\mathrm{F}^{(**)} + 0.83\mathrm{BC} + 0.30\,\mathrm{BD} + 0.10\mathrm{BE} + 0.43\mathrm{CD} + 1.03\mathrm{CE} - 0.84\,\mathrm{DE} + 3.66\,\mathrm{B}^2(*) + 0.29\,\mathrm{D}^2 - 0.72\,E^2 \quad \text{Eq 4.1}$$

*Variables in the equation follow the symbols reported in table 4.1 of fabrication protocol

Initially, procedural parameters have been selected on the base of the previous experience gained working with different plasmonic paper SERS substrates, trying to figure out which were the most important parameters to optimize the acquisition of SERS CSPP serum spectra. Thus, we have selected six procedural steps to produce the CSPP protocols. The procedural parameters are reported in **table 4.1**. In the order, a first drying time step has been performed after serum addition, because it be supposed to help fixing the serum on the paper and to slight concentrate the analyte on it. As second step the volume of colloids into the Eppendorf tube was selected to roughly match the serum level on the strip. Successively, serum spotted strips were incubated 20 minutes in the colloidal nanoparticles, with the idea to favouring the serum-spotted paper NPs

interaction. Centrifugation time and speed was arbitrary set to 10 minute and 4300xg, respectively. As final step, before spectra acquisition, serum sample drying (20 minutes) was performed, as we observed that water is negatively impacting spectra acquisition from plasmonic paper.

All these parameters were studied with a specific experimental design to understand how their variation impacts the CSPP serum SERS spectra and to evaluate the possible interactions among them. Thus, a linear regression model, which equation is reported as Eq. 4.1 was performed and validated, as described in the method section. Specifically, we have selected two different response variables: the normalized AUC of Uric Acid band and the normalized AUC at 1020-1080 $cm^{-1}$, a Raman band due to the cellulose background. therefore, the model was made with only 21 experimental conditions over the all 216 of a full factorial design, thanks to a d-optimal algorithm implementation [28]. The model was able to fit our data demonstrating that only two parameters significantly impact the measurements (from those reported in table 4.1): the drying time after centrifugation and the centrifugation time.

Specifically, a Pareto graph is reported in **Figure 4.3** (panel a) to display which procedural parameters (run in table S11) have the better response, considering the two variables simultaneously. Thus, the Pareto front (red line) shows the conditions with higher metabolite intensity and low cellulose background. Particularly, runs' 8 and 19 spectra that lay on the Pareto front, are reported in **Figure 4.3**, b panel. These two sets of conditions exhibit the highest levels of centrifugation and drying time, in line with the outcome of the linear model.

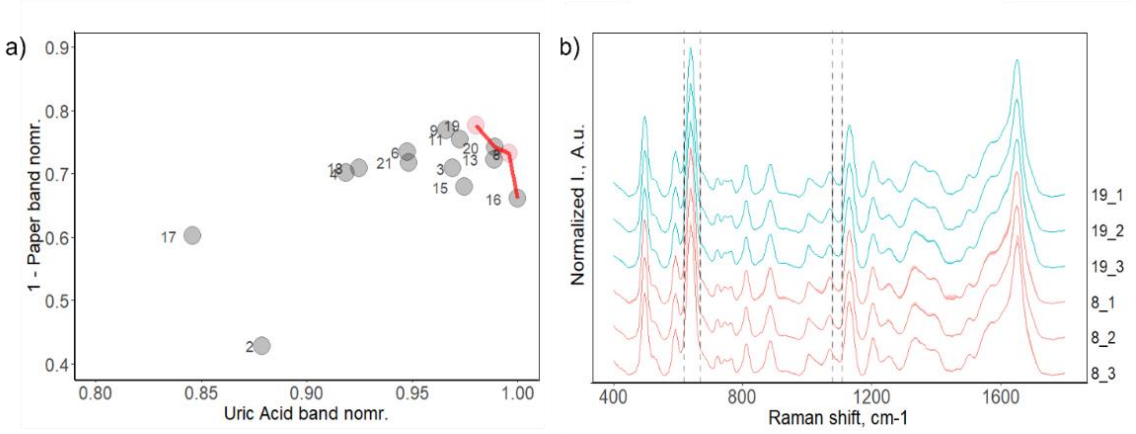


**Figure 4.3** model validation dataset. a) Pareto front of D-optimal selected run, in function of the two Y of linear regression models showing as dominating point runs that improve goodness of SERS spectra. Red line, dominating point; red dots, validation dataset runs; grey non dominating point. b) median and IQR

SERS spectra of validation dataset, aggregated per single CSPP. In this way Intra-substrate variation is visually shown. Run 19, cyan; run 8, red. Dashed line delimited in the order uric acid and cellulose Raman band region.

Hence, to definitively prove the effect of this parameters *ad hoc* experiments, outside the experimental design, have been performed. Normalized spectra are reported in **Figure 4.3** (panel a, c). Therefore, for an easier comprehension dot plot are reported (panel b, d) also, showing the effect on uric acid band. As expected, A clear increment of the intensity on the uric acid band is obtained by rising drying and centrifugation time. In addition, in line with the model prediction, the noise level and the Raman cellulose band at 1020-1080 $cm^{-1}$ drastically decrease rising the drying time.

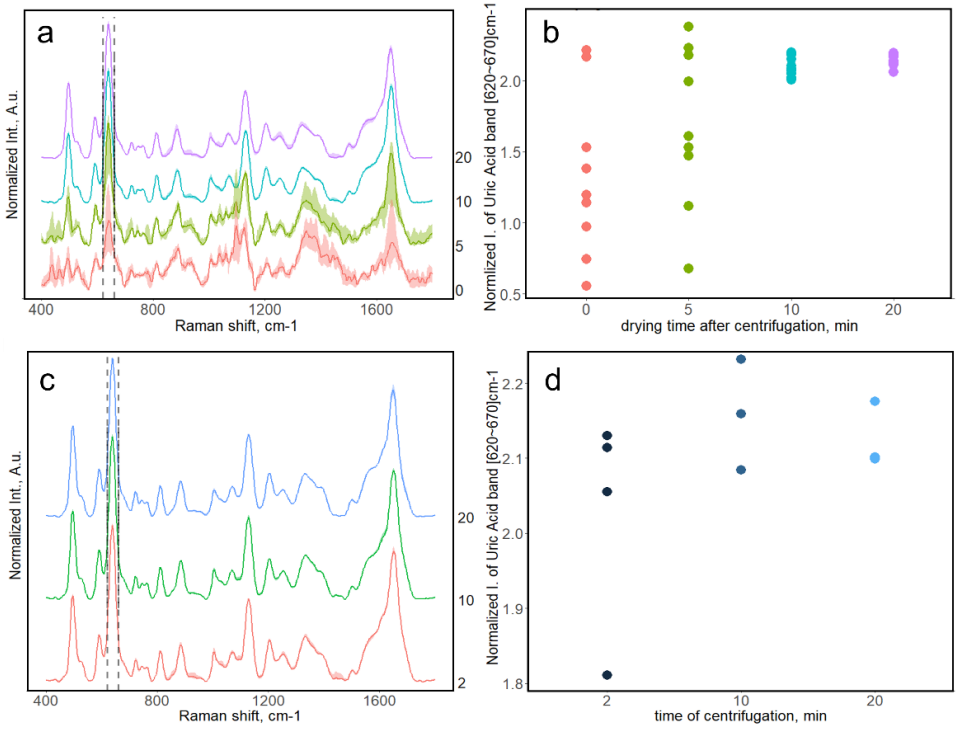


***Figure 4.4*** SERS spectra of CSPP sampling protocol influencing parameters. a) SERS spectra of CSPP whit different drying time after centrifugation from 0 up to 20 minutes. b) dot plot of uric acid band integrated area over different drying time. c) SERS spectra of CSPP whit 3 different time of centrifugation from 2 up to 20 minutes. d) dot plot representation of uric acid band Integrated area variation in response to different centrifugation time. 216, 384,720, 1000

The optimized protocol obtained by the linear regression model was used to verify the system variability. Hence, 10 CSPPs have been measured, with 10 spectra each to assess spectral variability. As method variability we refer to the RSD intra-CSPP. Looking at processed data, a method RSD of 40% can be assessed on unnormalized spectra, even if a reduction to less of 10% has been reached with normalized data. This

discrepancy can be conducted to the centrifugation process. As possible evidence, on CSPP at least two areas with different morphology can be found, as shown in **Figure 4.5**. Therefore, these two morphologies are related to a different distribution of nanoparticles, as showed in SEM images (b and c panel **figure 4.5**), showing probably regions with different SERS enhancement due to variation of SERS hot-spots formation. However, the hot-spots formation and distribution is not the only issue to be considered. The areas with a high concentration of nanoparticles can exhibit photodegradation problems, reducing the SERS enhancement and introducing artefacts in the spectra, accounting on the base of the experimental observations. Thus, the hot spot variability along the strip led us to introduce a high number of intra-CSPP replicates to overcome this issue, while deformed spectra were discarded in presence of high level of NPs aggregate or on the strip edges.

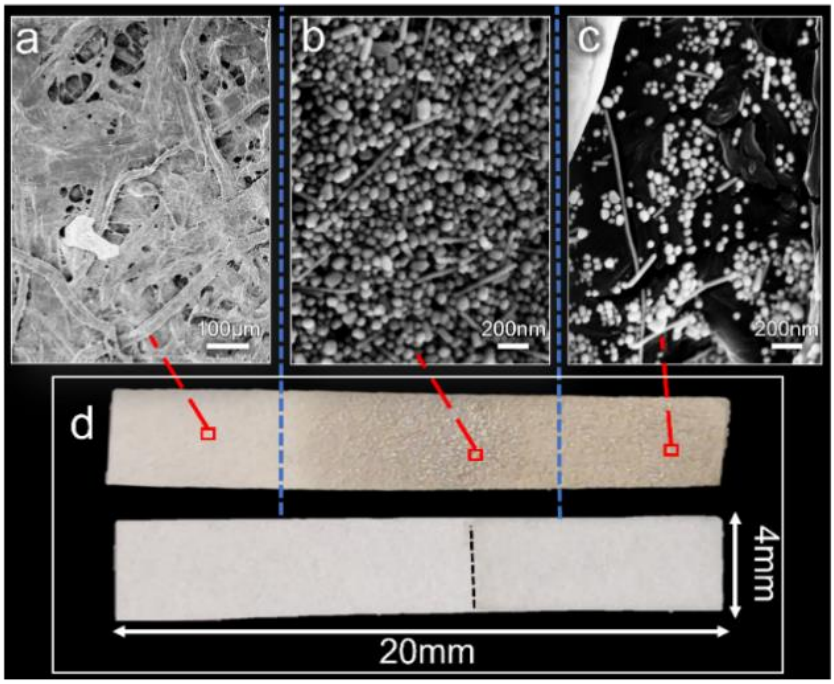


***Figure4.5*** CSPP and SEM cAg NPs distribution on paper: a, b, and c SEM images of CSSP after centrifugation of three different levels of Nanoparticle density; d paper strip after serum spotting (bottom) and after centrifugation with colloidal Ag NPs (top), on it are visible three different levels of grey intensity corresponding to the different densities of NPs on the strip reported in SEM images (separated with dashed blue lines). The dashed black line shows the level of serum on the strip.

Considering the substrates' inhomogeneity, we expect that unnormalized data show a high variability in the intensity of SERS serum spectra. On the contrary, relative intensity of bands in normalized spectra show a low variability (in terms of relative standard deviation, RSD). To explain the reduction of the variability of normalized

spectra, can be supposed that signal variability can be mainly mediated by hot-spot variability, more likely related to signal intensity, that is accommodated with the normalization. On the contrary no theories can be formulated about the modalities of the serum distribution along the strip, since by simple looking at the protein distribution with colorimetric test (e.g., blue Coomassie paper staining) has not be possible appreciate a specific pattern distribution (data not shown). To investigate this aspect more specifically biomolecular analysis are needed, that are beyond the aim of this study. However, the low RSD of relative intensities indicates the method capability in capture changes in the relative amount of serum metabolites, thus the CSPP method could be a good candidate for many label-free bio-analytical applications where the absolute intensity is not crucial.

On the other hand, the high repeatability of the normalized serum spectra could also imply that the CSPP methodology might be insensible to the subtle changes in relative metabolites concentrations, usually observed in the subjects involved in diagnostic or prognostic studies. To assess this hypothesis, two pure metabolites often observed in SERS spectra of biofluids, hypoxanthine and ergothioneine [27] have been used to spike serum samples in different amounts to simulate biochemical differences linked to a physiological condition, and the spiked samples were analysed with the CSPP protocol. Intense SERS spectra of these metabolites have been produced in serum showing the main SERS bands of the two probing metabolites, clearly resembling the SERS spectra previously reported in literature [17] [21]. Even with the concentrations of 10 μM and 5 μM for the ergothioneine and the hypoxanthine, respectively, we were able to see slight increments of specific metabolites' bands (data not shown) .

However, a PCA (principal component analysis) have been performed to assess if were possible to differentiate among the serum blank spectra and those spiked with metabolites, on the base of the spectral variability [18]. The results are presented in Appendix A figure S14 showing a clear separation among the three classes (serum; serum + Erg.; serum + Hyp.) by looking at the score plot of PC1-PC2 components. This separation has been obtained with 50 μM of hypoxanthine and 25 μM of ergothioneine, whose spectra are reported in **figure 6**, indicating the possibility to clearly detect metabolite changing in concentration into the micromolar order.

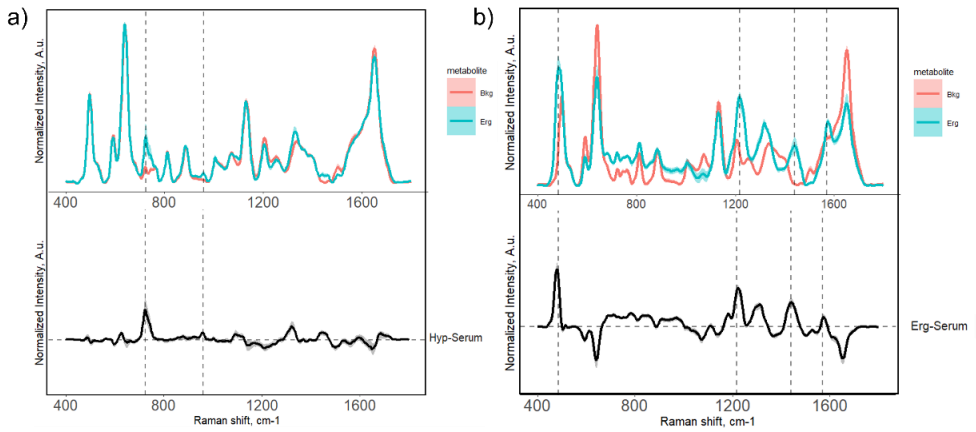


***Figure 6*** SERS spectra of CSPP of pure components in serum. median spectra and IQR a) top, over imposed spectra of serum and serum + 50 $\mu$M hypoxanthine, in red and cyan respectively; bottom difference spectrum hypoxanthine-serum. b) top, over imposed spectra of serum and serum+ 25 $\mu$M ergothioneine, in red and cyan respectively; bottom, difference spectrum ergothioneine -serum. a) and b), dashed lines, main peaks of pure metabolite spiked in serum.

Discriminate through different relevant biological metabolites and theirs concentrations is the main scope of a reliable bio-analytical method; to the same extent, to prove the reliability of our system as sampling method, it is indispensable to assess the stability of the dry serum spotted on the paper over time. Since we have developed a paper collecting support for SERS bio-analytical purposes, the shelf-life of spotted serum strips have been tested up to two months (as reported in the method section), as CSPP serum signal. Interestingly, no distortions of the spectral information were occurred during all the tested period, showing high repeatability of the normalized intensity over the time also. Instead, a slight decrease of the absolute intensity occurred after one month of storage. It is shown in **figure 7**, where the SERS signal is reported over the time and specifically, into dot plot as integrated area of the intensity of the main uric acid band to show the trend. Overall, these results permit a certain degree of freedom in collection and SERS analysis scheduling. In fact, due to the stability of the

signal, larger label-free SERS sampling campaign even on global scale are possible, thanks to the easiness of transportation of paper spotted strips also.

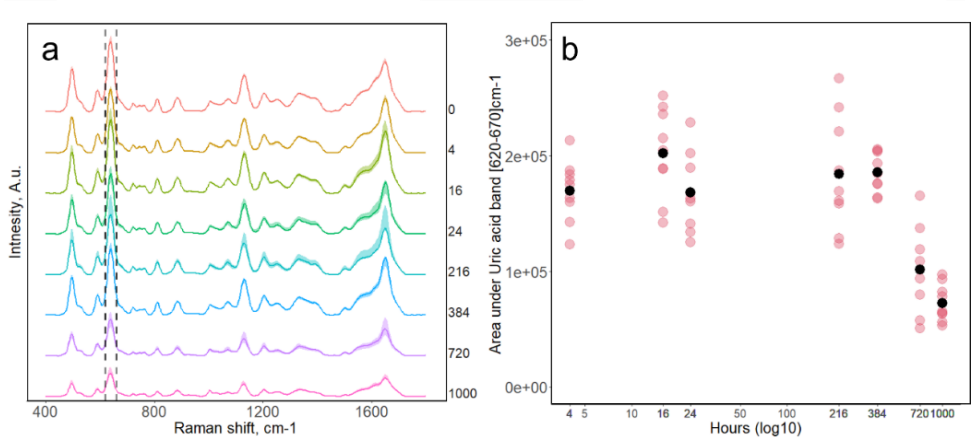


***Figure 4.7*** shelf-life evaluation of serum for CSPP sampling protocol. a) median and IQR SERS spectra of different aliquots of serum stored on the paper over the time, reported in hours on the right. dashed line, uric acid band b) dot plot reporting uric acid band integrated area over the time in log scale. In red, single strip; in black, mean values.

**Conclusions**

Plasmonic paper is a wide world in SERS substrates fabrication field: many protocols have been proposed and for various applications [11]. The general aims of plasmonic papers production is to reduce the cost of substrates, even often the reproducibility is reduced; to simplify the procedure of solid substrates fabrication; and finally, to facilitate on spot SERS applications.

Aside from the reproducibility, that is a common issue in this kind of substrates, a more general drawback, affecting all paper SERS application, is production throughput. This aspect is an important limiting factor in the commercialization, [11] considering also that each protocol can be applied for a unique of few applications. Thus, plasmonic paper remains at laboratory scale level still. Eventually, even in biomedical fields, SERS is far from real clinical applications. The difficult interpretation of SERS data, driven by a lack of a unique theoretical approach and by an arduous accordance among the data obtained with different SERS substrates, are the main limitations to introduce SERS in clinics.

In this context, our work has tried to reduce the gap in plasmonic paper production throughput, pointing on a sampling methodology based on a unique centrifugal step. Thus, before the collection of the sample no former paper treatment is necessary. In this way we have chosen a sampling methodology, rather than to produce

a SERS analytical method based on plasmonic paper only. Furthermore, centrifugation process allows to overcome the problems related to the protein corona in colloidal substrates and eliminates the needing of a serum filtration step. This aspect, together with the high similarity of spectral information obtained by other SERS substrates (e.g., colloids, gold solid substrate, dip-coated plasmonic paper, see figure S15 in Appendix A), make CSPP methodology a reliable protocol for SERS biosensing of biofluids. Finally, it also provides that metabolic fingerprinting exhibited by SERS label-free application has solid experimental bases.

## Bibliography


1. Ding, S.-Y.; Yi, J.; Li, J.-F.; Ren, B.; Wu, D.-Y.; Panneerselvam, R.; Tian, Z.-Q. Nanostructure-Based Plasmon-Enhanced Raman Spectroscopy for Surface Analysis of Materials. *Nat Rev Mater* **2016**, *1*, 16021, doi:10.1038/natrevmats.2016.21.
2. Kumar, G.V.P. Plasmonic Nano-Architectures for Surface Enhanced Raman Scattering: A Review. *J. Nanophoton* **2012**, *6*, 064503, doi:10.1117/1.JNP.6.064503.
3. Turkevich, J.; Stevenson, P.C.; Hillier, J. A Study of the Nucleation and Growth Processes in the Synthesis of Colloidal Gold. *Discuss. Faraday Soc.* **1951**, *11*, 55, doi:10.1039/df9511100055.
4. Lee, P.C.; Meisel, D. Adsorption and Surface-Enhanced Raman of Dyes on Silver and Gold Sols. *J. Phys. Chem.* **1982**, *86*, 3391–3395, doi:10.1021/j100214a025.
5. Premasiri, W.R.; Moir, D.T.; Klempner, M.S.; Krieger, N.; Jones, G.; Ziegler, L.D. Characterization of the Surface Enhanced Raman Scattering (SERS) of Bacteria. *J. Phys. Chem. B* **2005**, *109*, 312–320, doi:10.1021/jp040442n.
6. Hasi, W.-L.-J.; Lin, X.; Lou, X.-T.; Lin, S.; Yang, F.; Lin, D.-Y.; Lu, Z.-W. Chloride Ion-Assisted Self-Assembly of Silver Nanoparticles on Filter Paper as SERS Substrate. *Appl. Phys. A* **2015**, *118*, 799–807, doi:10.1007/s00339-014-8800-x.
7. Goodacre, R.; Graham, D.; Faulds, K. Recent Developments in Quantitative SERS: Moving towards Absolute Quantification. *TrAC Trends in Analytical Chemistry* **2018**, *102*, 359–368, doi:10.1016/j.trac.2018.03.005.
8. Tantra, R.; Brown, R.J.C.; Milton, M.J.T. Strategy to Improve the Reproducibility of Colloidal SERS. *J. Raman Spectrosc.* **2007**, *38*, 1469–1479, doi:10.1002/jrs.1797.
9. Linh, V.T.N.; Moon, J.; Mun, C.; Devaraj, V.; Oh, J.-W.; Park, S.-G.; Kim, D.-H.; Choo, J.; Lee, Y.-I.; Jung, H.S. A Facile Low-Cost Paper-Based SERS Substrate for Label-Free Molecular Detection. *Sensors and Actuators B: Chemical* **2019**, *291*, 369–377, doi:10.1016/j.snb.2019.04.077.
10. Dalla Marta, S.; Novara, C.; Giorgis, F.; Bonifacio, A.; Sergo, V. Optimization and Characterization of Paper-Made Surface Enhanced Raman Scattering (SERS) Substrates with Au and Ag NPs for Quantitative Analysis. *Materials* **2017**, *10*, 1365, doi:10.3390/ma10121365.

11. Mekonnen, M.L.; Su, W.-N.; Chen, C.-H.; Hwang, B.-J. Ag@$SiO_2$ Nanocube Loaded Miniaturized Filter Paper as a Hybrid Flexible Plasmonic SERS Substrate for Trace Melamine Detection. *Anal. Methods* **2017**, *9*, 6823–6829, doi:10.1039/C7AY02192E.

12. Zhang, R.; Xu, B.-B.; Liu, X.-Q.; Zhang, Y.-L.; Xu, Y.; Chen, Q.-D.; Sun, H.-B. Highly Efficient SERS Test Strips. *Chem. Commun.* **2012**, *48*, 5913, doi:10.1039/c2cc31604h.

13. Polavarapu, L.; Liz-Marzán, L.M. Towards Low-Cost Flexible Substrates for Nanoplasmonic Sensing. *Phys. Chem. Chem. Phys.* **2013**, *15*, 5288, doi:10.1039/c2cp43642f.

14. Mekonnen, M.L.; Workie, Y.A.; Su, W.-N.; Hwang, B.J. Plasmonic Paper Substrates for Point-of-Need Applications: Recent Developments and Fabrication Methods. *Sensors and Actuators B: Chemical* **2021**, *345*, 130401, doi:10.1016/j.snb.2021.130401.

15. Cheng, H.; Yi, L.; Wu, J.; Li, G.; Zhao, G.; Xiao, Z.; Hu, B.; Zhao, L.; Tian, J. Drug Preconcentration and Direct Quantification in Biofluids Using 3D-Printed Paper Cartridge. *Biosensors and Bioelectronics* **2021**, *189*, 113266, doi:10.1016/j.bios.2021.113266.

16. Kim, W.-S.; Shin, J.-H.; Park, H.-K.; Choi, S. A Low-Cost, Monometallic, Surface-Enhanced Raman Scattering-Functionalized Paper Platform for Spot-on Bioassays. *Sensors and Actuators B: Chemical* **2016**, *222*, 1112–1118, doi:10.1016/j.snb.2015.08.030.

17. Li, H.; Wang, Q.; Tang, J.; Gao, N.; Yue, X.; Zhong, F.; Lv, X.; Fu, J.; Wang, T.; Ma, C. Establishment of a Reliable Scheme for Obtaining Highly Stable SERS Signal of Biological Serum. *Biosensors and Bioelectronics* **2021**, *189*, 113315, doi:10.1016/j.bios.2021.113315.

18. Bonifacio, A.; Cervo, S.; Sergo, V. Label-Free Surface-Enhanced Raman Spectroscopy of Biofluids: Fundamental Aspects and Diagnostic Applications. *Anal Bioanal Chem* **2015**, *407*, 8265–8277, doi:10.1007/s00216-015-8697-z.

19. Belaites C., Sergo V. "hyperSpec: A Package to Handle Hyperspectral Data Sets in R", R Package Version 0.98-20161118. [(accessed on 30 September 2017)]; Available online: http://hyperspec.r-forge.r-project.org

20. Wickham, H. *Ggplot2: Elegant Graphics for Data Analysis*; Use R!; 2nd ed. 2016.; Springer International Publishing : Imprint: Springer: Cham, 2016; ISBN 978-3-319-24277-4.

21. R. Leardi, C. Melzi, G. Polotti, CAT (Chemometric Agile Tool), freely downloadable from http://gruppochemiometria.it/index.php/software

22. Fornasaro, S.; Berton, F.; Stacchi, C.; Farina, F.; Esposito, A.; Sergo, V.; Di Lenarda, R.; Bonifacio, A. Label-Free Analysis of Gingival Crevicular Fluid (GCF) by Surface Enhanced Raman Scattering (SERS). *Analyst* **2021**, *146*, 1464–1471, doi:10.1039/d0an01997f.

23. Fornasaro, S.; Gurian, E.; Pagarin, S.; Genova, E.; Stocco, G.; Decorti, G.; Sergo, V.; Bonifacio, A. Ergothioneine, a Dietary Amino Acid with a High Relevance for the Interpretation of Label-Free Surface Enhanced Raman Scattering (SERS) Spectra of Many Biological Samples. *Spectrochimica Acta Part A: Molecular and Biomolecular Spectroscopy* **2021**, *246*, 119024, doi:10.1016/j.saa.2020.119024

24. Premasiri, W.R.; Lee, J.C.; Ziegler, L.D. Surface-Enhanced Raman Scattering of Whole Human Blood, Blood Plasma, and Red Blood Cells: Cellular Processes and Bioanalytica

25. Lin, D.; Pan, J.; Huang, H.; Chen, G.; Qiu, S.; Shi, H.; Chen, W.; Yu, Y.; Feng, S.; Chen, R. Label-Free Blood Plasma Test Based on Surface-Enhanced Raman Scattering for Tumour Stages Detection in Nasopharyngeal Cancer. *Sci Rep* **2015**, *4*, 4751, doi:10.1038/srep04751.

26. Gurian, E.; Di Silvestre, A.; Mitri, E.; Pascut, D.; Tiribelli, C.; Giuffrè, M.; Crocè, L.S.; Sergo, V.; Bonifacio, A. Repeated Double Cross-Validation Applied to the PCA-LDA Classification of SERS Spectra: A Case Study with Serum Samples from Hepatocellular Carcinoma Patients. *Anal Bioanal Chem* **2021**, *413*, 1303–1312, doi:10.1007/s00216-020-03093-7.

27. Zhang, Z.-M.; Liu, J.-F.; Liu, R.; Sun, J.-F.; Wei, G.-H. Thin Layer Chromatography Coupled with Surface-Enhanced Raman Scattering as a Facile Method for On-Site Quantitative Monitoring of Chemical Reactions. *Anal. Chem.* **2014**, *86*, 7286–7292, doi:10.1021/ac5017387.

28. Li, B.; Zhang, W.; Chen, L.; Lin, B. A Fast and Low-Cost Spray Method for Prototyping and Depositing Surface-Enhanced Raman Scattering Arrays on Microfluidic Paper Based Device: Microfluidics and Miniaturization. *ELECTROPHORESIS* **2013**, *34*, 2162–2168,10.1007/s00216-010-3739-z.

29. Siebe, H.S.; Chen, Q.; Li, X.; Xu, Y.; Browne, W.R.; Bell, S.E.J. Filter Paper Based SERS Substrate for the Direct Detection of Analytes in Complex Matrices. *Analyst* **2021**, *146*, 1281–1288, doi:10.1039/D0AN02103B.

30. Jang, W.; Byun, H.; Kim, J.-H. Rapid Preparation of Paper-Based Plasmonic Platforms for SERS Applications. *Materials Chemistry and Physics* **2020**, *240*, 122124, doi:10.1016/j.matchemphys.2019.122124.

31. Jarvis, R.M.; Rowe, W.; Yaffe, N.R.; O'Connor, R.; Knowles, J.D.; Blanch, E.W.; Goodacre, R. Multiobjective Evolutionary Optimisation for Surface-Enhanced Raman Scattering. *Anal Bioanal Chem* **2010**, *397*, 1893–1901, doi:10.1007/s00216-010-3739-z.

# 5. Conclusions

The aim of my entire PhD project has been to research and develop new biofluids investigation methods, with a label-free SERS approach. the SERS biosensing is a valuable and fruitful method to obtain biochemical information form biofluid, as reported in several literature references and shown in all the course this thesis dissertation. It is a powerful tool for the simplicity of its implementation in terms of cost and time expenditure, and generally it consists in poor or no sample processing, and few seconds of measurement acquisition for each spectrum.

But the process to develop a label-free SERS methodology is rather far to be a simple task, since SERS signal is obtained with a synergic strategy related to plasmonic efficiency of the nanostructured materials, the metabolites affinity for the metal and the biochemical environment at the nano-bio interface. Thus, label-free modality is the simplest approach that does not require labelling or reporter molecules and any surface functionalization, but many experimental aspects can influence the result. Counterintuitively, this can be considered as a flexibility factor, rather than a limiting one. In fact, by changing the experimental conditions we can move toward a different pool of molecules of interest, at the same extent of adding a filter to a picture to emphasize certain specific aspects. For instance, we can improve the binding of a class of metabolite and reduce the affinity for others, by acting on biochemical parameters like pH and ionic strength.

On the other hand, the affinity of chemical moieties for the plasmonic surface and its geometry remain less tunable factors. Thus, before to move toward an experimental design approach (in which biochemical factors must be fully considered) is convenient a more routinary approach to use readily available SERS substrate to assess the metabolic “profile” of different biological matrices. This aspect led us to try to develop a system for stool samples analysis: simple methanolic faecal extract mixed with colloidal nanoparticles produced a stable and intense signal.

This has suggested us, as natural consequence, to investigate with the SERS the gut metabolome. Especially, for the last two decades research on gut metabolome and the gut bacteria has been emerging as a precious source of information on the general

health state of patient, in biomedicine [6]. Eventually, metabolomic analytical procedure are complex and expansive and SERS can help to reduce the gap between standard highly cost analysis, like mass spectroscopy, and routine biomedical analysis.

Particularly, the case of the celiac disease we presented in the previous chapter has shown that SERS metabolic biosensing in stool samples can be used to solve unmet clinical issues, even on a limited pool of metabolites and once properly validate. Specifically, At the best of our knowledge, our data suggest the possibility to follow the compliance of GFD to the diet, by looking at the hypoxanthine level that has shown a dramatic increment in this class of patients. Moreover, fully understand why and which are the biological reasons for a biochemical change in the level of hypoxanthine in gluten free diet patients is far to be understood and is beyond the label-free SERS potentialities. However, from the merely bioanalytical point of view, the data has underlined clearly a specific metabolic difference among the class of patients, that, by itself, is a remarkable result and need to be proven with a larger sample size.

The second part of the thesis was devoted to developing a faster procedure to obtain serum SERS signal on paper substrates, and to produce a reliable SERS sampling system: the CSPP methodology. In this case a simple process was used to extract the SERS signal of the serum absorbed on paper strips. Specifically, the paper support was supposed to be used as a sampling device, and the SERS signal is obtained by centrifugation with colloidal silver nanoparticles, which decorate the paper and strongly interact with the metabolic components of the serum. This process has shown to be able with very simple approach to reduce the protein corona effect (responsible for hindering the hot-spot formation) by favouring the interaction with serum metabolite, such as the uric acid that seems to interact in a preferential way with the colloidal nanoparticles during the centrifugation. On the other hand, spiking the serum with micromolar concentration of ergothioneine and hypoxanthine have shown that other metabolites can be analysed with this methodology. On whole, the method has provided high reproducibility and signal stability even after two months of serum spotted papers storage, permitting long and diffused measurement campaign. This allowed to rise the number of available simples, favouring more reliable results, that positively impacting on the label-free SERS application reproducibility, that generally suffer of high variability

# Appendix A: supplementary materials

In this appendix are reported the supplementary materials for chapter 3 and 4.

| class | sex | age |
|---|---|---|
| C | F | 7 |
| C | M | 10 |
| C | M | 4 |
| C | M | 6 |
| C | M | 7 |
| C | F | 10 |
| C | F | 10 |
| C | M | 5 |
| CD | F | 16 |
| CD | M | 14 |
| CD | F | 3 |
| CD | F | 3 |
| CD | F | 4 |
| CD | M | 13 |
| CD | F | 16 |
| CD | F | 10 |
| CD | F | 6 |
| GFD | F | 12 |
| GFD | M | 14 |
| GFD | M | 9 |
| GFD | F | 12 |
| GFD | F | 12 |
| GFD | F | 16 |
| GFD | F | 17 |
| GFD | F | 13 |
| GFD | F | 12 |
| GFD | M | 24 |

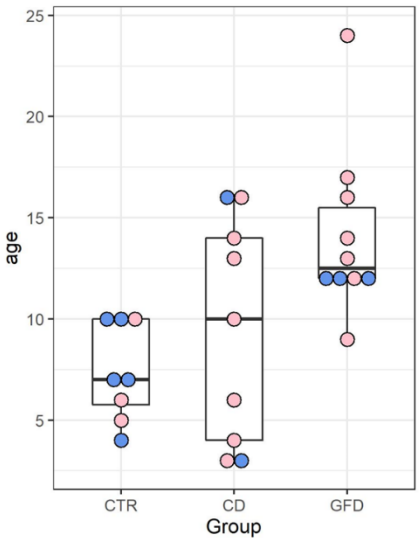


**Figure S1**: (left) characteristics (age, sex) of the subjects participating to the study. In the boxplot (right) blue dot = male, pink dot = female.

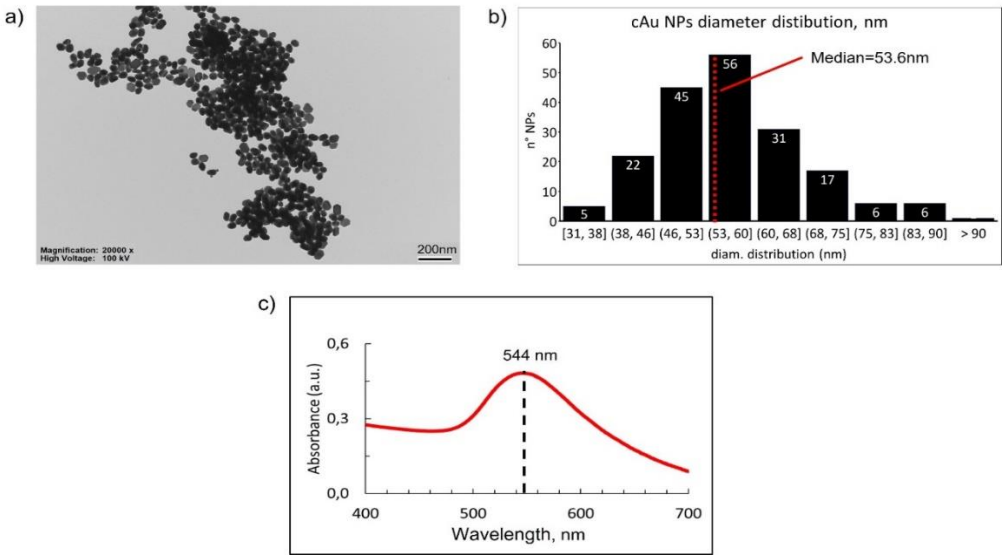


**Figure S2.** Characterization of AuNP: a) TEM image of AuNP, b) size distribution of AuNP as derived from TEM, c) Visible extinction spectrum of the colloidal dispersion of AuNP (10-fold diluted).

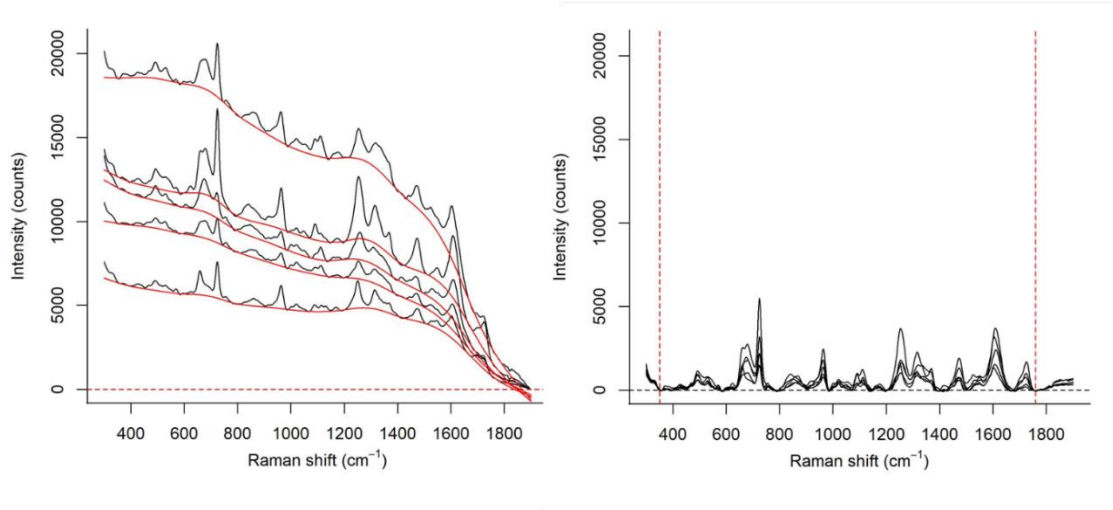


**Figure S3**: Examples of baseline subtraction and spectral range cropping shown for a random selection of 5 spectra from the dataset (see Methods section of the main manuscript for details).

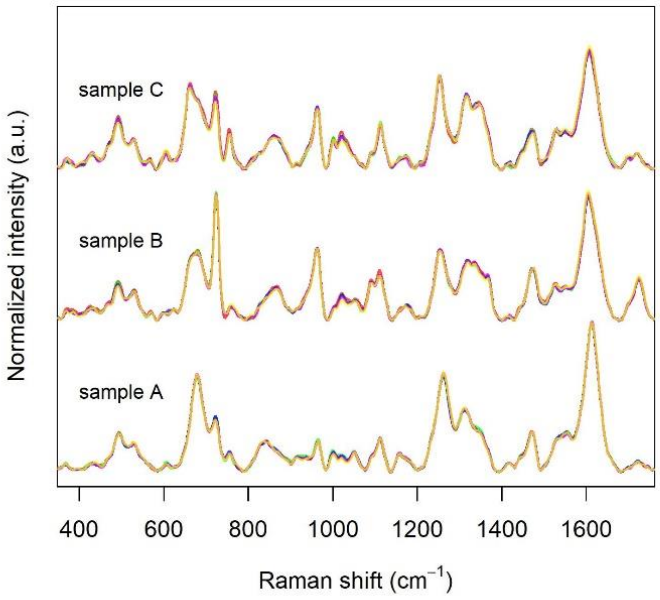


**Figure S4**: replicates of SERS spectra (from 5 aliquots of the faecal extract) for 3 randomly selected samples. Spectra have different colors and are overlaid, showing a high repeatability of SERS measurements. Excitation wavelength 785 nm, AuNP used as SERS substrate.

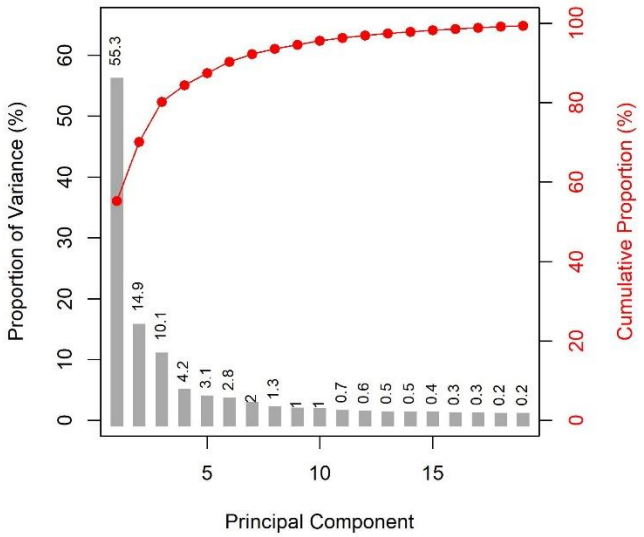


**Figure S5**: Proportion of variance and cumulative proportion of variance explained for the first 19 principal components according to the PCA.

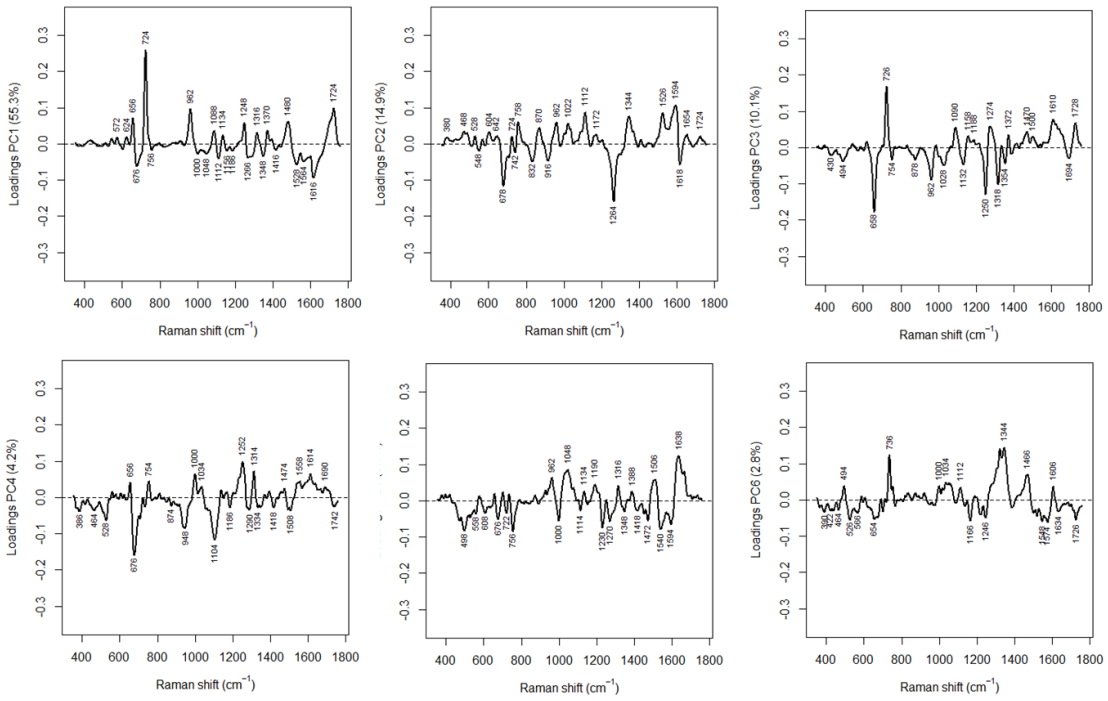


**Figure S6**. Loadings of the first six principal components of the SERS dataset.

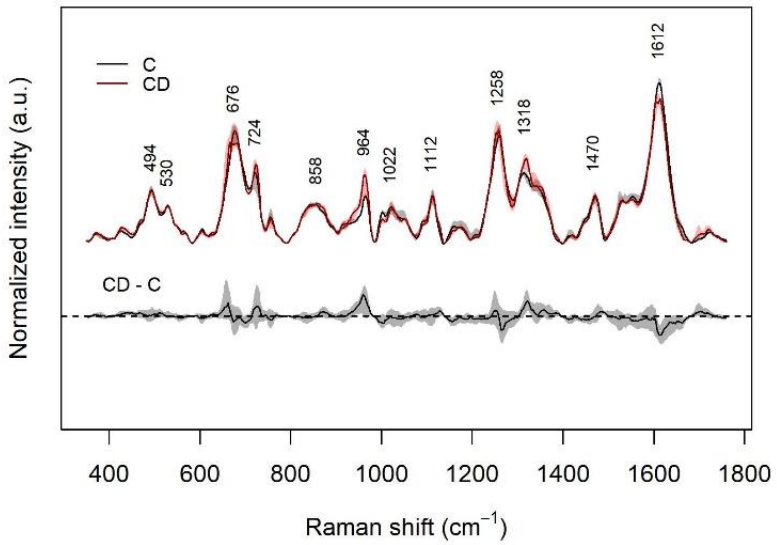


**Figure S7**. Comparison between medians and interquartiles (shaded areas) of the intensity for the SERS spectra of the celiac disease (CD, red) and controls (C, blue) groups, together with the median and interquartile of all the difference spectra (black). Excitation wavelength 785 nm, AuNP used as SERS substrate

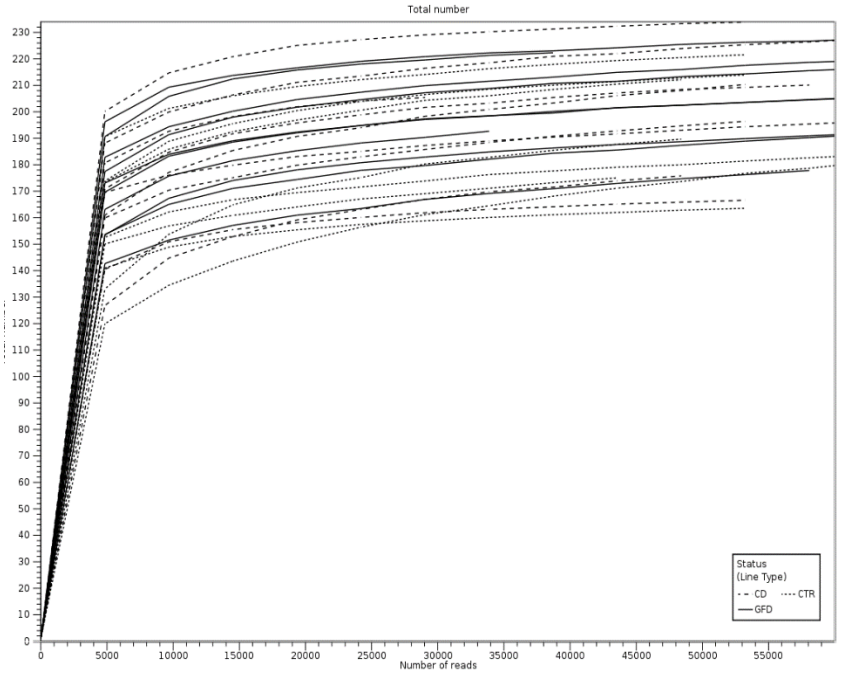


**Figure S8**. Rarefaction curves calculated for total OTUs abundance

| Name | Max group mean | Log2 fold change | Fold change | p-value | FDR p-value |
|---|---|---|---|---|---|
| *Uncultured bacterium* (order Mollicutes) | 447.67 | -11.33 | -2582.15 | <0.001 | **<0.001** |
| *Akkermansiaceae* (order Verruvomicrobiales) | 1369.44 | -7.42 | -170.97 | <0.001 | **<0.001** |
| *Clostridiaceae 1* (order Clostridiales) | **2315.33** | **-2.98** | **-7.88** | **0.020** | **0.020** |

**Table S9**. Results from a Differential Abundance Analysis (GFD vs. CD). Only the bacterial families with a Bonferroni-corrected p-value ≤ 0.05 are shown.

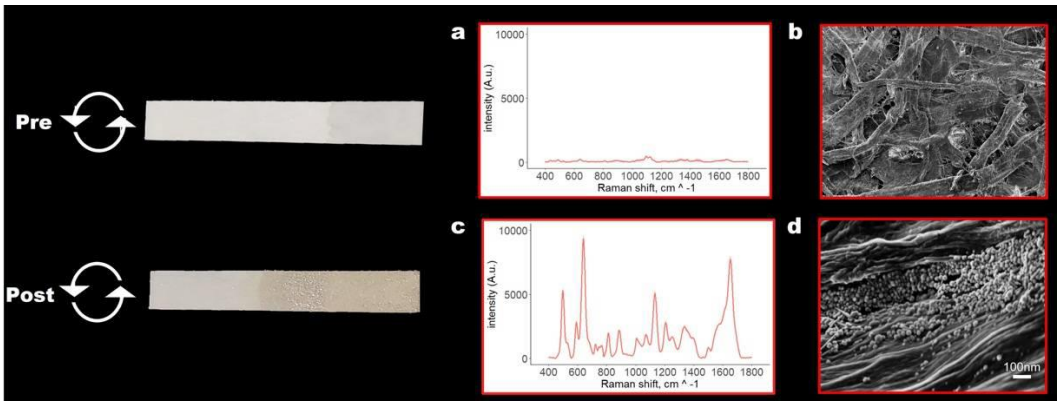


**Figure S10** Serum-soaked paper strip before and after centrifugation; (a, c), SERS spectra; (b, d) SEM images.

| SET | $t_{dry}$ (min) | $V_{col}$ (µL) | $t^{inc}$ (min) | $t_{cent}$ (min) | s (rpm) | $t_{dry2}$ (min) | A (min) | B (µL) | C (min) | D (min) | E (rpm) | F (min) | Y |
|---|---|---|---|---|---|---|---|---|---|---|---|---|---|
| | 20 | 150 | 0 | 2 | 4000 | 0 | 1 | 1 | -1 | -1 | -1 | -1 | 2.01 |
| | 0 | 75 | 0 | 2 | 13000 | 0 | -1 | -1 | -1 | -1 | 1 | -1 | 5.21 |
| | 20 | 150 | 0 | 20 | 4000 | 0 | 1 | 1 | -1 | 1 | -1 | -1 | 9.11 |
| | 0 | 75 | 20 | 2 | 4000 | 20 | -1 | -1 | 1 | -1 | -1 | 1 | 8.64 |
| | 20 | 150 | 0 | 2 | 13000 | 0 | 1 | 1 | -1 | -1 | 1 | -1 | 0.84 |
| | 0 | 75 | 0 | 20 | 4000 | 0 | -1 | -1 | -1 | 1 | -1 | -1 | 10.44 |
| | 20 | 100 | 0 | 2 | 4000 | 20 | 1 | -0.3 | -1 | -1 | -1 | 1 | 5.40 |
| | 20 | 75 | 0 | 10 | 8000 | 20 | 1 | -1 | -1 | -0.11 | -0.11 | 1 | 11.33 |
| | 0 | 75 | 20 | 20 | 13000 | 0 | -1 | -1 | 1 | 1 | 1 | -1 | 9.00 |
| | 0 | 100 | 0 | 10 | 13000 | 0 | -1 | -0.3 | -1 | -0.11 | 1 | -1 | 0.74 |
| M | 20 | 75 | 0 | 20 | 13000 | 20 | 1 | -1 | -1 | 1 | 1 | 1 | 8.56 |
| | 20 | 75 | 20 | 10 | 4000 | 0 | 1 | -1 | 1 | -0.11 | -1 | -1 | 3.84 |
| | 0 | 150 | 0 | 20 | 8000 | 20 | -1 | 1 | -1 | 1 | -0.11 | 1 | 9.53 |
| | 20 | 100 | 20 | 10 | 8000 | 0 | 1 | -0.3 | 1 | -0.11 | -0.11 | -1 | 3.05 |
| | 0 | 150 | 0 | 10 | 13000 | 20 | -1 | 1 | -1 | -0.11 | 1 | 1 | 8.48 |
| | 20 | 150 | 20 | 20 | 13000 | 0 | 1 | 1 | 1 | 1 | 1 | -1 | 9.11 |
| | 0 | 150 | 20 | 2 | 8000 | 0 | -1 | 1 | 1 | -1 | -0.11 | -1 | 7.23 |
| | 0 | 150 | 20 | 10 | 4000 | 20 | -1 | 1 | 1 | -0.11 | -1 | 1 | 10.09 |
| | 20 | 100 | 20 | 20 | 4000 | 20 | 1 | -0.3 | 1 | 1 | -1 | 1 | 10.05 |
| | 20 | 75 | 20 | 2 | 13000 | 20 | 1 | -1 | 1 | -1 | 1 | 1 | 8.95 |
| | 20 | 150 | 20 | 2 | 13000 | 20 | 1 | 1 | 1 | -1 | 1 | 1 | 9.22 |
| | 0 | 75 | 20 | 2 | 4000 | 20 | -1 | -1 | 1 | -1 | -1 | 1 | 8.44 |
| V | 20 | 75 | 0 | 10 | 8000 | 20 | 1 | -1 | -1 | -0.11 | -0.11 | 1 | 9.48 |
| | 20 | 100 | 20 | 20 | 4000 | 20 | 1 | -0.3 | 1 | 1 | -1 | 1 | 9.53 |
| | 20 | 75 | 20 | 2 | 13000 | 20 | 1 | -1 | 1 | -1 | 1 | 1 | 9.05 |

**Table S11** Experimental matrix reporting the 25 experiments performed, with the sequence of values applied for the six experimental factors and their correspondent range-scaled X variable (A-F), in the D-optimal design for CSPP optimization. M, experimental runs; V, validation runs; Y, response variable (UA/cellulose ratio). tdry, analyte drying time; Vcol, Ag-NPs volume;tinc, incubation time; tcent, centrifugation time; s, centrifugation speed; tdry2, drying time after centrifugation.

| EXP | PRED | lev | $CI_{95\%}$ | res |
|---|---|---|---|---|
| 8.44 | 7.97 | 0.77 | 4.16 - 11.78 | -0.47 |
| 9.48 | 10.49 | 0.79 | 6.63 - 14.35 | 1.01 |
| 9.53 | 9.51 | 0.88 | 5.44 - 13.58 | -0.02 |
| 9.05 | 9.20 | 0.74 | 5.48 - 12.93 | 0.16 |

**Table S12** Results of model validation. EXP, experimental value; PRED, model prediction; lev, leverage; LLCI, CI95%, confidence interval at 95%; res, residuals.

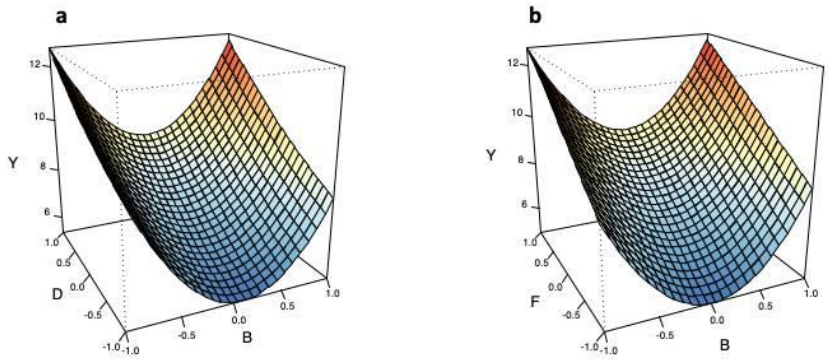


**Figure S13** Response surfaces. a) Response (Y) predicted by the experimental design model as a function of D (centrifugation time) and B (volume of colloidal AgNPs solution), while keeping A =0 (10 min), C = 0 (10 min), E = 0 (8000 rpm), and F= 1 (20 min); b). Response (Y) predicted by the experimental design model as a function of F (drying time after centrifugation) and B (volume of colloidal AgNPs solution), while keeping A = 0 (10 min), C = 0 (10 min), D= 1 (20 min), and E = 0 (8000 rpm).

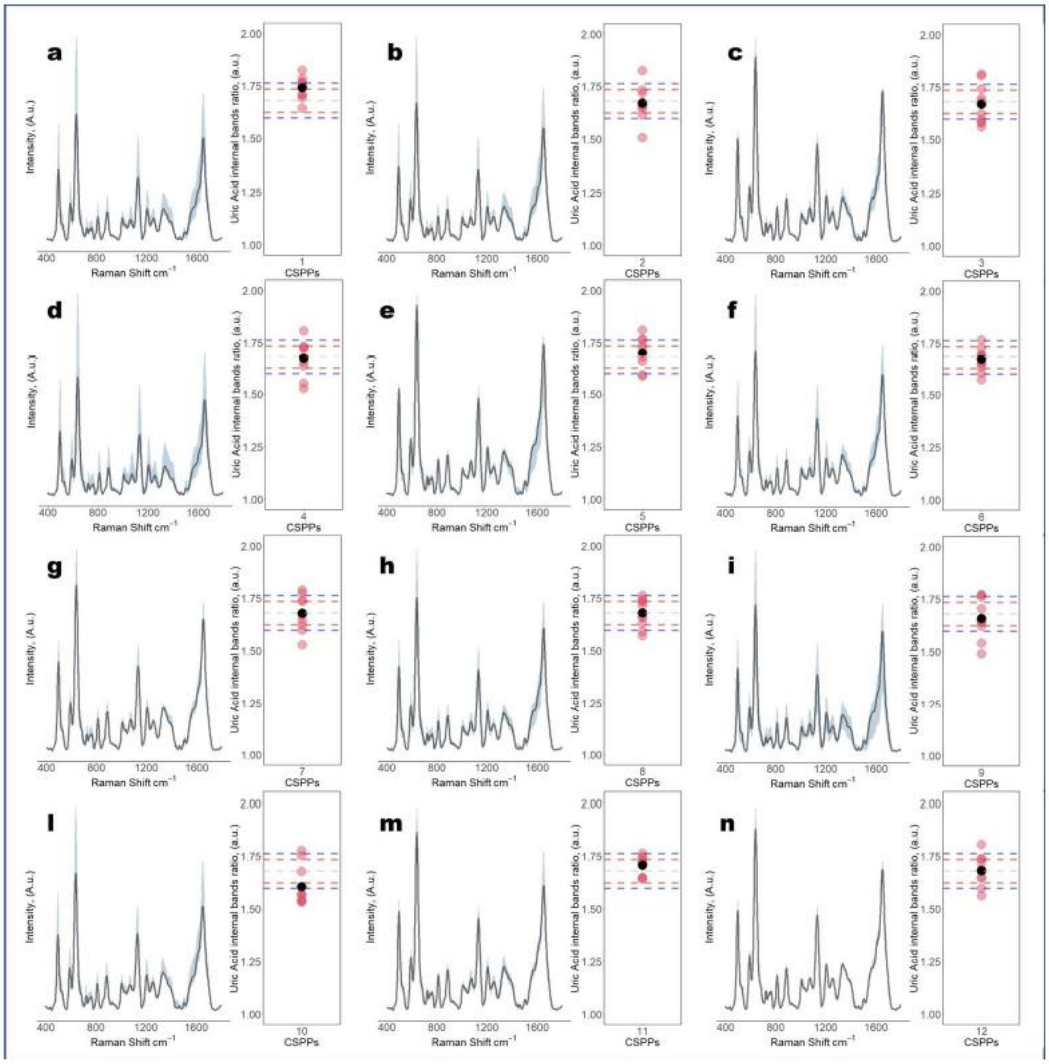


**Figure S14.** Reproducibility of the CSPP method (n=12). Black dots correspond to the mean value for the ratio between the 640 (skeletal ring deformation) and 1132 (C-N) cm-1 bands of uric acid of 10 randomly chosen positions on the same CSPP. The red shaded lines span the interquartile range (IQR), calculated over the entire set of measurements, corresponding to the range covered by 50% of the data. The dashed blue lines mark the median and the extremes of the acceptance area (1.5 x IQR).

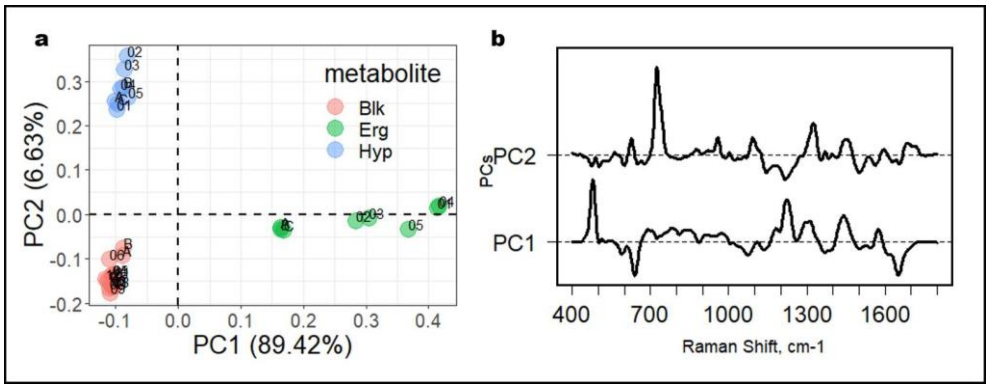


**Figure S15** Principal components analysis. a) PC1-PC2 score plot of the dataset used in section. b) variable loadings profiles on PC1 and PC2. Blk, human serum; Erg, serum spiked with 25 µM ergothioneine; Hyp, human serum spiked with 50 µM hypoxanthine.

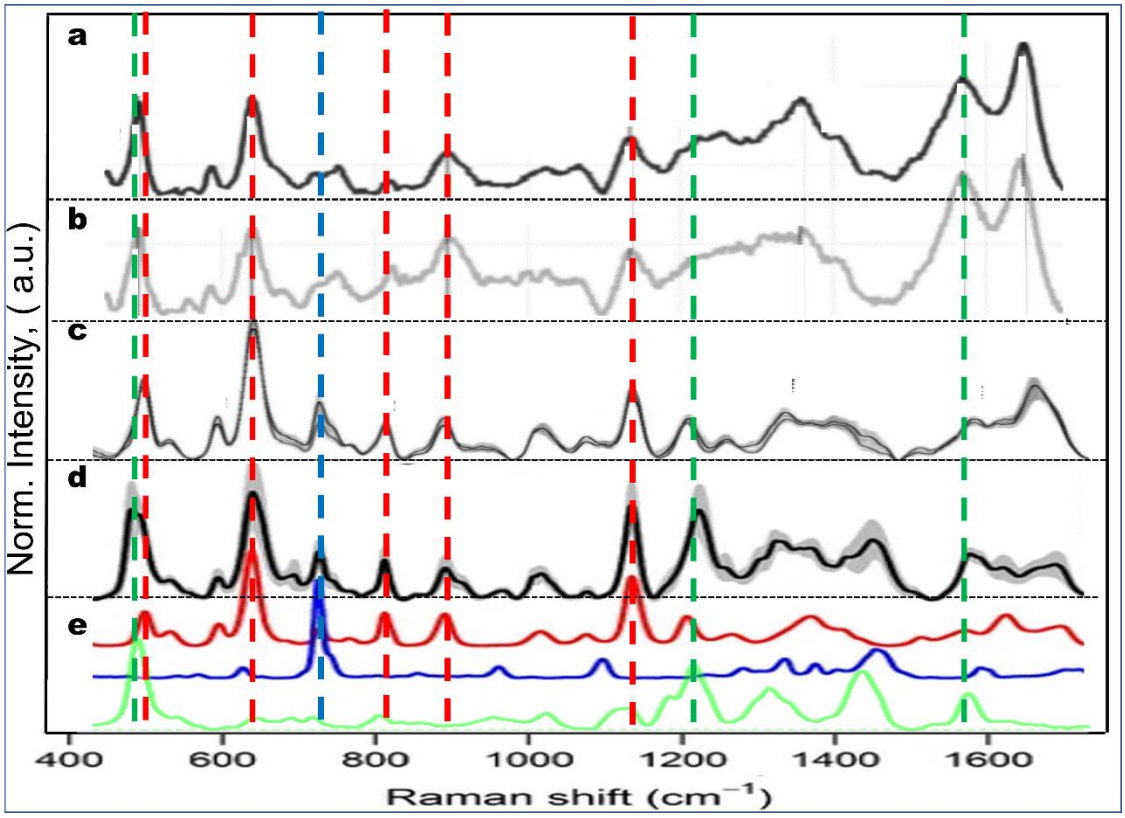


**Figure S16** comparison of SERS spectra obtained from Human serum and plasma obtained forma from different references in literature and with different SERS substrates (a-d). and compared with pure metabolites in (e), uric acid, hypoxanthine and ergothioneine, respectively in red, blue and green.